Cao *et al. Advances in Aerodynamics* (2025) 7:19
https://doi.org/10.1186/s42774-025-00230-7

Advances in Aerodynamics

RESEARCH Open Access

Double time-relaxation kinetic model for compressible turbulence modeling

Guiyu Cao[1,2*], Liang Pan[3], Kun Xu[4] and Shiyi Chen[2*]

*Correspondence:
guiyu.cao@eng.ox.ac.uk;
chensy@sustc.edu.cn

[1] Department of Engineering Science, University of Oxford, Oxford, UK
[2] Academy for Advanced Interdisciplinary Studies, Southern University of Science and Technology, Shenzhen 518055, China
[3] Laboratory of Mathematics and Complex Systems, School of Mathematical Sciences, Beijing Normal University, Beijing 100875, China
[4] Department of Mathematics, The Hong Kong University of Science and Technology, Hong Kong, China

Abstract

In this paper, a double time-relaxation kinetic model (DtrKM) is proposed for compressible turbulence modeling on unresolved grids. Within the double time-relaxation framework, DtrKM is extended in the form of generalized Bhatnagar-Gross-Krook model. Based on the first-order Chapman-Enskog expansion, DtrKM connects with the six-variable macroscopic governing equations. The first five governing equations correspond to the conservative laws in mass, momentum and total energy, while the sixth equation governs the evolution of unresolved turbulence kinetic energy K_{utke}. The unknowns in DtrKM, including turbulent relaxation time and source term, are modeled via gradient-type assumption and standard dynamic modeling approach. The current kinetic model on unresolved grids correspondingly offers a mesoscopic understanding for one-equation subgrid-scale turbulence kinetic energy K_{sgs} model for compressible large eddy simulation. To solve DtrKM accurately and robustly, a high-accuracy gas-kinetic scheme is developed, which inherits the advantages of well-established gas-kinetic scheme for simulating macroscopic governing equations. Three-dimensional decaying compressible isotropic turbulence and temporal compressible plane mixing layer on unresolved grids are simulated to evaluate the generalized kinetic model. The performance of key turbulent quantities up to second-order statistics confirms that DtrKM is comparable with the widely-used dynamic Smagorinsky model. The DtrKM provides a workable approach for compressible turbulence modeling and simulation on unresolved grids.

Keywords: Kinetic model, Double relaxation, Compressible turbulence modeling, High-accuracy gas-kinetic scheme

1 Introduction

Turbulence modeling on unresolved grids is a challenging issue in turbulence community for decades [1]. With the rapid increasing of computational power, the large eddy simulation (LES) [2, 3] gradually becomes the tractable workhorse for high-fidelity turbulence simulation. To simulate turbulent flows on unresolved grids, LES solves the filtered Navier-Stokes (NS) equations with resolvable large-scale turbulent structures explicitly, while the unresolved structures are modeled through subgrid-scale (SGS) models [4, 5]. The widely-used eddy-viscosity LES models in physical space mainly include zero-equation Smagorinsky-class models and one-equation SGS turbulence kinetic energy models [6, 7].

Smagorinsky model (SM) proposed by Manabe et al. [2] belongs to zero-equation eddy-viscosity model. SM models unresolved turbulent structures through gradient-type assumption between the SGS stress and the resolved velocity gradient. In practice, SM requires to adjust empirical coefficients according to the flow types, and suffers the over-dissipative performance near the wall. Additionally, SGS effect of SM does not disappear in the laminar flow region [8]. To deal with those flaws of the SM, dynamic Smagorinsky model (DSM) [9–12] has been proposed and developed for incompressible and compressible turbulence modeling. DSM allows the modeling coefficients to be computed locally at each time step on the basis of dynamic approaches, namely, the coefficient calculated based upon two filterings of the flow variables.

Another branch to model the unresolved turbulent structures is deriving and modeling SGS turbulence kinetic energy (TKE). Schumann, Yoshizawa and Horiuti [6, 7] have pioneered one-equation SGS turbulence kinetic energy model to incorporate historical and non-local effects via transport equation of SGS turbulence kinetic energy K_{sgs}. The one-equation SGS turbulence kinetic energy model can be analogous to the one-equation Reynolds averaged Navier-Stokes eddy-viscosity model [13]. As the grid filter width is taken as the characteristic modeling length scale, only the SGS turbulence kinetic energy equation is required to determine the eddy viscosity. One-equation SGS turbulence kinetic energy models have been extensively applied in incompressible LES [14, 15]. Compared with the well-established research on compressibility correction for the unresolved TKE equation in the RANS simulation [13, 16], there only exists limited work on one-equation SGS turbulence kinetic energy models for compressible LES [17–20]. Considering that the compressibility effects can be modeled in the evolution of TKE, it is reasonable to explore the benefits of one-equation SGS turbulence kinetic energy model.

In the past decades, the gas-kinetic scheme (GKS) and the high-order gas-kinetic scheme (HGKS) based on the Bhatnagar-Gross-Krook (BGK) model [21, 22] have been developed systematically for the computations from low speed flows to hypersonic ones [23, 24]. GKS presents a gas evolution process from kinetic scale to hydrodynamic scale, where both inviscid and viscous fluxes are recovered from a time-dependent and genuinely multi-dimensional gas distribution function at a cell interface. In discontinuous shock region, the kinetic scale particle transport physics takes effect to construct a crisp and stable shock transition. In smooth flow region, the accurate Navier-Stokes solution can be obtained once the flow structure is well resolved. For HGKS, to achieve the high-order spatial accuracy and the robustness, the classical WENO reconstruction [25] is adopted. For the temporal discretization, the two-stage fourth-order method is used, as fourth-order temporal accuracy can be achieved within two-stages, and the efficiency can be also improved.

Within the kinetic framework, Hou et al. and Chen et al. [26, 27] pioneered the turbulent relaxation time τ_t for BGK-type models in turbulence modeling. Following the concept of turbulent relaxation time, second-order GKS and HGKS have been implemented in simulating turbulent flows, especially in the compressible regime. For practical high-Reynolds number turbulent flows, the second-order GKS/HGKS coupled with $k-\omega$ SST model [28–30], S-A model [31], and the hybrid RANS-LES method [32] have been performed in simulating high-Reynolds number turbulence. These high-Reynolds

number practical simulations have confirmed the accuracy and robustness of second-order GKS/HGKS coupled with traditional eddy-viscosity model. Recently, the kinetic Fokker–Planck equation [33] and the multi-scale wave-particle model [34] have been proposed for turbulence, which pave the workable approaches for the kinetic turbulence modeling.

In terms of low-Reynolds number turbulent flows, the second-order GKS/HGKS have been directly used as a direct numerical simulation (DNS) or LES tool in simulating the canonical benchmarks [35–39], such as compressible mixing layer, compressible homogeneous turbulence, turbulent channel flows, etc. HGKS shows unique advantages in the supersonic turbulence due to its accuracy and super robustness [20]. Within the time-relaxation framework, to construct one-equation SGS turbulence kinetic energy model which preserves the non-local and historical effects for compressible LES, Cao et al. [20, 39] have systematically studied the high-fidelity DNS and implemented delicate *a priori* coarse-graining analysis on decaying compressible isotropic turbulence.

This paper aims to complete the compressible one-equation K_{sgs} model for LES under the time-relaxation kinetic framework, and to assess its effectiveness via the *a posteriori* performance. Firstly, double time-relaxation kinetic model (DtrKM) is extended in the form of modified BGK model. DtrKM can offer a mesoscopic understanding for transport equation of the compressible SGS turbulence kinetic energy. To inherit the accurate and robust numerical performance of HGKS, a finite volume high-accuracy gas-kinetic scheme for DtrKM is designed, where the WENO reconstruction and the two-step fourth-order time discretization are used to improve the spatial-temporal accuracy when solving DtrKM. Comparable with the widely-used eddy-viscosity DSM, the decaying compressible isotropic turbulence (DCIT) [39, 40] and temporal compressible plane mixing layer (TCPML) [41–43] are simulated to evaluate the current generalized kinetic model and the corresponding high-accuracy gas-kinetic scheme.

The organization of this paper is as follows. In Section 2, DtrKM for compressible turbulence modeling is presented. Section 3 constructs the finite volume high-accuracy gas-kinetic scheme for DtrKM. *A posteriori* numerical tests on DCIT and TCPML are conducted in Section 4. Conclusion and discussion are presented in Section 5.

2 Double time-relaxation kinetic model for compressible turbulence modeling

In this section, we firstly present DtrKM on unresolved grids. The first-order Chapman-Enskog expansion bridges the DtrKM and corresponding macroscopic governing equations with six macroscopic variables. Phenomenologically, the unknown turbulent relaxation time and source term are modeled through the gradient-type assumption and dynamic modeling approach, which are well defined in the NS framework.

2.1 Bhatnagar-Gross-Krook time-relaxation kinetic model

For molecular transport and collision, the simplification of Boltzmann equation without external force is given by the BGK model [21],

$$\frac{\partial f}{\partial t}+u_i\frac{\partial f}{\partial x_i}=\frac{g-f}{\tau}, \tag{1}$$

where $f(\boldsymbol{x}, t, \boldsymbol{u}, \xi)$ is the number density of molecules at position $\boldsymbol{x} = (x_1, x_2, x_3)^T$ and molecular velocity $\boldsymbol{u} = (u_1, u_2, u_3)^T$ at time t with internal degrees of freedom ξ. The relation between distribution function $f(\boldsymbol{x}, t, \boldsymbol{u}, \xi)$ and macroscopic variables, such as mass, momentum and total energy, can be obtained by taking moments in molecular velocity of $f(\boldsymbol{x}, t, \boldsymbol{u}, \xi)$ [23, 24]. The left hand side of BGK model denotes the free transport process, and the right hand side is the time-relaxation collision term. The collision term in BGK model shows simple relaxation process from $f(\boldsymbol{x}, t, \boldsymbol{u}, \xi)$ to a local equilibrium state g, with a molecular relaxation time τ which is related to the molecular viscosity μ and the heat conduction coefficient κ (see Appendix 2 [24]). The local equilibrium state g is a Maxwellian distribution,

$$g = \rho\left(\frac{\lambda}{\pi}\right)^{\frac{N+3}{2}} e^{-\lambda\left[(u_i-U_i)^2+\xi^2\right]}, \tag{2}$$

where ρ is the density, $\lambda = m_o/(2k_BT)$ as m_o is the molecular mass, k_B the Boltzmann constant and T the temperature, and U_i denotes the macroscopic velocity in the x_i direction. For three-dimensional equilibrium diatomic gas, the total number of degrees of freedom in ξ is $N = 2$, accounting for the two rotational modes $\xi^2 = \xi_1^2 + \xi_2^2$. The specific heat ratio γ is determined by $\gamma = (N + 5)/(N + 3)$. Zeroth-order Chapman-Enskog expansion [22] with $f = g$ offers the Euler equations. NS equations can be derived with first-order truncation of Chapman-Enskog expansion,

$$f = g - \tau\left(\frac{\partial g}{\partial t} + u_i\frac{\partial g}{\partial x_i}\right). \tag{3}$$

For Euler and NS equations, the second-order and high-order GKS based on BGK model (see Eq. (1)) has been systematically developed [23, 44]. The well-established second-order GKS/HGKS presents its accurate and robust numerical performance from low speed flows to hypersonic ones [24].

2.2 Double time-relaxation kinetic model

Numerically, the resolved state or unresolved state on a numerical cell depends on the ratio of spatial-temporal resolution of numerical simulation to the local characteristic scale of flow field. DNS resolves full scales above Kolmogorov scale, eliminating turbulence models entirely. Unresolved grids definitely lead to the loss of turbulent information due to the inevitable space and time averaging process when updating the macroscopic variables (similar to the averaging process in the finite volume scheme [24]). The key point for turbulence modeling is to model the unresolved turbulence structure through additional non-trivial quantities on unresolved grids, i.e., non-trivial turbulent frequency governed by the stochastic differential equation [1]. The trivial quantities are mass, momentum and total energy, which are governed by the conservative laws, without contributing non-trivial information to the unresolved turbulent structures. Subsequently, on unresolved grids, the non-trivial unresolved turbulence kinetic energy K_{utke} and its quantitative dynamic evolution will be proposed for modeling the unresolved turbulence.

To model turbulence on unresolved grids, the double time-relaxation kinetic model is proposed in the form of modified BGK model,

$$\frac{\partial f}{\partial t}+u_i\frac{\partial f}{\partial x_i}=\frac{f^{eq}-f}{\tau+\tau_t}+\frac{g-f^{eq}}{\tau_*}\equiv\frac{f^{eq}-f}{\tau+\tau_t}+Q_s, \tag{4}$$

where $f(\boldsymbol{x},t,\boldsymbol{u},\xi,k_u)$ is the generalized number density of molecules on unresolved grids, k_u the sample-space variable corresponding to unresolved TKE K_{utke}, τ_t the turbulent relaxation time, τ_* the newly-defined relaxation time from f^{eq} to g, and Q_s the secondary relaxation term. Turbulence equilibrium state f^{eq} is introduced with Maxwellian distribution g for resolved flow variables and Gamma distribution gk_u for unresolved TKE as

$$f^{eq}=g\cdot gk_u=\rho\left(\frac{\lambda}{\pi}\right)^{\frac{N+3}{2}}e^{-\lambda[(u_i-U_i)^2+\xi^2]}\cdot\frac{1}{\Gamma(\alpha)}\left(\frac{\alpha}{K_{utke}}\right)^{\alpha}k_u^{\alpha-1}e^{-\frac{\alpha k_u}{K_{utke}}}, \tag{5}$$

where $\cdot$ denotes the multiplication. We assume $gk_u(k_u)$ is the Gamma distribution, with non-negative shape parameter α, mean $Mean(k_u)=K_{utke}$, variance $Var(k_u)=K_{utke}^2/\alpha$, where K_{utke} is the total unresolved TKE on unresolved grids. Thence, the double-relaxation process is named as double time-relaxation kinetic model, as the unresolved turbulence information K_{utke} participates in the double relaxation process.

In Jayesh-Pope model [1], Gamma distribution is the stationary distribution of turbulence frequency for statistically stationary isotropic turbulence. In DtrKM, the distribution of K_{utke} on unresolved grids is chosen as Gamma distribution (see Eq. (5)), intuitively. Validity of Gamma distribution on K_{utke} is conducted through the following coarse-graining process. Based on the previous DNS study on 384^3 grids [20], the distribution of K_{utke} through coarsening DNS solution is presented in Fig. 1. K_{utke} is normalized as 1 in Fig. 1. Gamma distribution with the parameter $\alpha=0.50$ is the canonical distribution. Gamma distribution equipped with the parameter $\alpha=0.39$ fits well with sample-space k_u from coarsening DNS data. In thick-tail region of Fig. 1, there exists apparent deviation between the fitted Gamma distribution and coarsening DNS data. This deviation implies that the intense events in the compressible isotropic turbulence [45] are hard to be modeled by Gamma distribution.

The optimal choice of distribution for K_{utke} on unresolved grids still requires to be investigated. However, the form of gk_u does not affect the evolution of K_{utke} with the subsequent finite volume high-accuracy gas-kinetic scheme. Since high-accuracy gas-kinetic scheme acts as a hydrodynamic solver, only the total K_{utke} gets involved in the updating process instead of k_u in Eq. (5). By contrast, when the kinetic solver is applied in updating the distribution function $f(\boldsymbol{x},t,\boldsymbol{u},\xi,k_u)$ directly on unresolved grids, i.e., unified gas-kinetic scheme (UGKS) [46], the form of gk_u will contribute to the evolution of $f(\boldsymbol{x},t,\boldsymbol{u},\xi,k_u)$. If DtrKM is solved by kinetic solver, the distribution of K_{utke} requires to be modeled much carefully. As a starter, turbulence equilibrium state f^{eq} (see Eq. (5)) has been proposed for constructing the non-trivial quantity on unresolved grid, namely, depicting the k_u for unresolved "turbulent eddies".

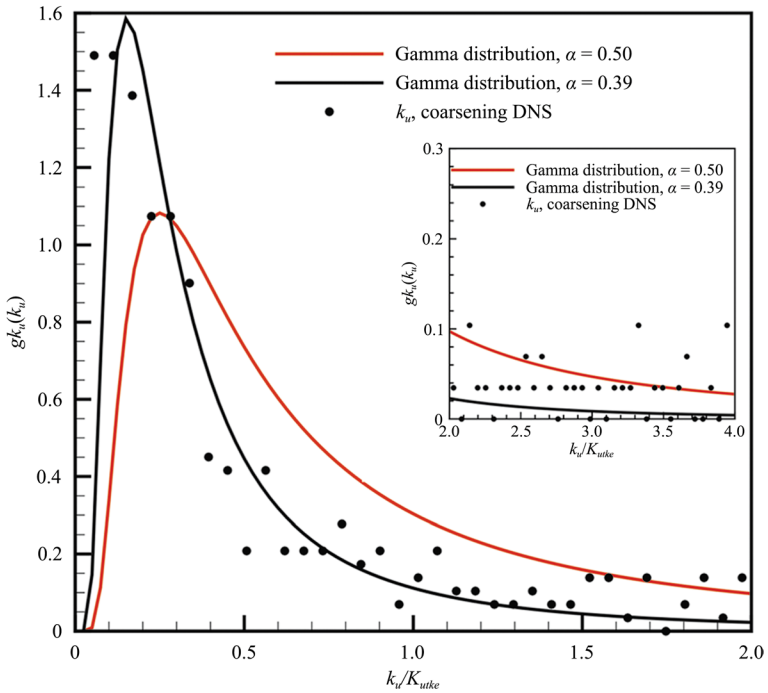

Fig. 1 $gk_U(k_U)$ from coarsening DNS [20] at $t/\tau_{tO} = 0.5$. 8^3 resolved grids are coarsened to 1 unresolved grid with a Box filter [47]. τ_{tO} is the large-eddy-turnover time

The relation between macroscopic variables, such as mass ρ, momentum $(\rho U_1, \rho U_2, \rho U_3)$, total energy ρE, and unresolved turbulence kinetic energy ρK_{utke} with the generalized distribution function $f(\boldsymbol{x}, t, \boldsymbol{u}, \xi, k_u)$ on unresolved grids is given by

$$\boldsymbol{Q} = \int \boldsymbol{\psi} f \, \mathrm{d}\Xi = (\rho, \rho U_1, \rho U_2, \rho U_3, \rho E, \rho K_{utke})^T, \tag{6}$$

where $\boldsymbol{\psi} = \left(1, u_1, u_2, u_3, \frac{1}{2}\left(u_1^2 + u_2^2 + u_3^2 + \xi^2\right) + k_u, k_u\right)^T$ and $\mathrm{d}\Xi = \mathrm{d}u_1 \mathrm{d}u_2 \mathrm{d}u_3 \mathrm{d}\xi \, \mathrm{d}k_u$. As the K_{utke} is introduced to model unresolved turbulent process quantitatively, one more constraint has to be imposed on the current DtrKM to self-consistently determine all unknowns. This additional constraint is the K_{utke} relaxation. Since only mass, momentum and total energy are conserved during collisions, the compatibility condition for the collision term becomes

$$\boldsymbol{S} = \int \boldsymbol{\psi} \left(\frac{f^{eq} - f}{\tau + \tau_t} + Q_s \right) \mathrm{d}\Xi = (0, 0, 0, 0, 0, S_t)^T. \tag{7}$$

Unknown source term S_t in Eq. (7) can be modeled through relaxation model. This relaxation process is analogous to the well-established non-equilibrium kinetic model for multi-temperature flows [48] as

$$S_t = \frac{\rho\left(K_{utke}^{eq} - K_{utke}\right)}{\tau_*}. \tag{8}$$

Conceptually, the equilibrium unresolved TKE K_{utke}^{eq} and relaxation time τ_* in Eq. (8) can be modeled on unresolved grids. However, these two unknowns require profound *a priori* knowledge and physical understanding of turbulence within the double time-relaxation framework. As far as the authors know, modeling K_{utke}^{eq} and τ_* in Eq. (8) directly is pretty challenging for current stage of turbulence studies. To overcome this barrier, a comparison between the ρK_{utke} equation derived from the first-order Chapman-Enskog expansion on DtrKM and the compressible K_{sgs} equation from the compressible LES [20] will be conducted. Consequently, source term S_t can be modeled in an alternative standard paradigm. After modeling S_t, the dynamic evolution of non-trivial quantity K_{utke} can be determined by Eqs. (4) and (7) quantitatively.

The double time-relaxation kinetic model for turbulence modeling on unresolved grids can be compared to the multiple temperature kinetic model for non-equilibrium flow computations [37, 48]. In contrast to the BGK model (1), the right-hand-side collision operator in DtrKM Eq. (4) contains two terms corresponding to two-level collisions on unresolved grids. The relaxation process has been extended as $f \to f^{eq} \to g$, and the process from $f^{eq} \to g$ may take a much longer time τ_* than that of the process from $f \to f^{eq}$ by $(\tau + \tau_t)$. On unresolved grids, for the first collision process, the information of unresolved K_{utke} is memorized by the intermediate turbulence equilibrium distribution f^{eq}; for the second collision process, K_{utke} is released into resolved kinetic energy and internal energy by τ_*. The total energy assignment in the two-level collision process can be classified as intermediate turbulence equilibrium state $\rho E = \rho \boldsymbol{U}^2/2 + \rho e + \rho K_{utke}$, and Maxwellian equilibrium state $\rho E = \rho \boldsymbol{U}^2/2 + \rho e$. $\boldsymbol{U} = (U_1, U_2, U_3)^T$ is the resolved macroscopic velocity vector with the definition of $\boldsymbol{U^2} = U_1^2 + U_2^2 + U_3^2$. $e = (N+3)RT/2$ is the internal energy, where R is the gas constant. As the unresolved grids approach resolved ones, the unresolved turbulent information tends to disappear, so the non-trivial modeling information on unresolved turbulence structures will be eliminated automatically. This limit implies $K_{utke} \to 0$, turbulent relaxation time $\tau_t \to 0$, turbulence equilibrium state $f^{eq} \to g$, and $\tau_* \to \tau$. Therefore, this limit leads the DtrKM in Eq. (4) to be consistent with the BGK model in Eq. (1) on resolved grids, without considering the subsequent modeling and numerical discretization errors. This asymptotic process also indicates that the turbulent relaxation time τ_t depends on grid resolution and unresolved K_{utke}, which sheds light on the modeling of the unknown turbulent relaxation time τ_t.

2.3 Chapman-Enskog expansion of DtrKM

To overcome the barrier of modeling the turbulent relaxation time τ_t and source term S_t directly in kinetic model, the corresponding macroscopic governing equations from the DtrKM will be derived by Chapman-Enskog expansion. DtrKM to macroscopic equations can be regarded as a projection, which essentially bridges the unknowns in DtrKM with the particular terms in macroscopic governing equations.

Using the turbulence equilibrium state denoted in Eq. (5), with the frozen K_{utke} exchange assumption, the first-order Chapman-Enskog expansion gives

$$f = f^{eq} - (\tau + \tau_t)\left(\frac{\partial f^{eq}}{\partial t} + u_i \frac{\partial f^{eq}}{\partial x_i}\right). \tag{9}$$

From which the corresponding macroscopic governing equations in three dimensions have been derived for the first time, as shown in Appendix 1, namely

$$\rho_{,t} + (\rho U_j)_{,j} = 0, \tag{10}$$

$$(\rho U_i)_{,t} + (\rho U_i U_j + p\delta_{ij})_{,j} = (\tau_{ij})_{,j}, \tag{11}$$

$$(\rho E)_{,t} + ((\rho E + p)U_j)_{,j} = (U_i \tau_{ij} + q_j)_{,j}, \tag{12}$$

$$(\rho K_{utke})_{,t} + (\rho K_{utke} U_j)_{,j} = (U_j \tau_{st} + qk_j)_{,j} + S_t, \tag{13}$$

where p is pressure related to the resolved temperature $p = \rho RT = \rho/(2\lambda)$, the total energy $\rho E = \rho(\boldsymbol{U}^2 + 3RT + NRT)/2 + \rho K_{utke}$, and δ_{ij} is the Kronecker symbol. The viscous stress term in Eq. (11) is denoted by

$$\tau_{ij} = (\mu + \mu_t)\left(U_{i,j} + U_{j,i} - \frac{2}{3}U_{k,k}\delta_{ij}\right) + \eta_t U_{k,k}\delta_{ij} - \frac{2}{N+3}\tau_{st}\delta_{ij}, \tag{14}$$

with

$$\tau_{st} = (\tau + \tau_t)S_t, \tag{15}$$

where molecular viscosity $\mu = \tau p$, turbulent eddy viscosity $\mu_t = \tau_t p$, turbulent bulk viscosity $\eta_t = 2N(\mu + \mu_t)/[3(N+3)]$, and the last term τ_{st} results from the source term S_t. Typically, beyond the filtered compressible momentum equation in NS equations [19], the generalized viscous stress τ_{ij} on unresolved grids in Eq. (14) contains additional terms. These terms are turbulent bulk viscosity term and term related to the energy interaction from source term S_t. Unresolved turbulence structure contributes to the generalized viscous stress so that τ_{ij} on unresolved grids deviates from the linear constitutive relation in Eq. (14). The heat conduction term in Eq. (12) reads

$$q_j = (\kappa + \kappa_t)T_{,j} + qk_j, \tag{16}$$

where molecular thermal conductivity is $\kappa = (N+5)\tau pR/2$, and turbulent thermal conductivity $\kappa_t = (N+5)\tau_t pR/2$. Appendix 1 shows that Prandtl number $Pr = 1$, and turbulent Prandtl number $Pr_t = 1$. When recovering the realistic laminar and turbulent Prandtl number, a similar modification in the energy transport [23] should be implemented. The modification will be presented briefly in Section 3. As presented in Eq. (13), the term qk_j is related to the governing equation of K_{utke} as

$$qk_j = (\mu + \mu_t)(K_{utke})_{,j}. \tag{17}$$

In summary, the first five governing equations in Eqs. (10)-(12) correspond to the conservative laws in mass, momentum and total energy with generalized constitutive relationship of stress in Eqs. (14)-(15) and heat conduction term in Eqs. (16)-(17). While the sixth Eq. (13) governs the evolution of K_{utke}. So far, the unclosed terms in DtrKM are the

turbulent relaxation time τ_t, and the source term S_t. In the following part, τ_t and S_t will be modeled through the comparison among Eqs. (10)-(13) and transport equations of the compressible SGS turbulence kinetic energy K_{sgs}.

2.4 Models for turbulent relaxation time τ_t and source term S_t

With the Favre filtering process (i.e., $\widetilde{U_i}$ denotes Favre average of U_i), the compressible $\overline{\rho}K_{sgs}$ transport equation [20] for compressible LES has been derived as

$$\begin{cases} \left(\overline{\rho}K_{sgs}\right)_{,t} + \left(\overline{\rho}K_{sgs}\widetilde{U}_j\right)_{,j} = P_{sgs} - D_{sgs} + \Pi_{sgs} + T_{sgs}, \\ P_{sgs} = -\tau_{ij}^{sgs}\widetilde{S}_{ij}, \\ D_{sgs} = \overline{\sigma_{ij}U_{i,j}} - \overline{\sigma}_{ij}\widetilde{U}_{i,j}, \\ \Pi_{sgs} = \overline{pU_{k,k}} - \overline{p}\widetilde{U}_{k,k}, \\ T_{sgs} = \left[-\frac{1}{2}\overline{\rho}\left(\widetilde{U_iU_iU_j} - \widetilde{U_i}\widetilde{U_i}\widetilde{U_j}\right) + \tau_{ij}^{sgs}\widetilde{U}_i \right. \\ \qquad \left. +(\overline{\sigma_{ij}U_i} - \overline{\sigma}_{ij}\widetilde{U}_i) - \overline{\rho}R\left(\widetilde{TU_j} - \widetilde{T}\widetilde{U}_j\right)\right]_{,j}, \end{cases} \tag{18}$$

where P_{sgs} is the production term, D_{sgs} the total dissipation term, Π_{sgs} the pressure-dilation transfer, and the last term T_{sgs} the sum of SGS diffusion terms. In Eq. (18), SGS turbulence kinetic energy $\overline{\rho}K_{sgs} = \tau_{kk}^{sgs}/2 = \overline{\rho}(\widetilde{U_kU_k} - \widetilde{U}_k\widetilde{U}_k)/2$, SGS stress $\tau_{ij}^{sgs} = \overline{\rho}(\widetilde{U_iU_j} - \widetilde{U}_i\widetilde{U}_j)$, $\widetilde{S}_{ij} = (\widetilde{U}_{i,j} + \widetilde{U}_{j,i})/2$, and $\sigma_{ij} = \mu\left(U_{i,j} + U_{j,i} - 2U_{k,k}\delta_{ij}/3\right)$. The total SGS dissipation rate D_{sgs} can be decomposed into two parts, namely, SGS solenoidal dissipation rate ε_s^{sgs} and SGS dilational dissipation rate ε_d^{sgs} as

$$\begin{cases} D_{sgs} = \epsilon_s^{sgs} + \epsilon_d^{sgs}, \\ \varepsilon_s^{sgs} = \overline{\mu}\left(\widetilde{\omega_i\omega_i} - \tilde{\omega}_i\tilde{\omega}_i\right), \\ \varepsilon_d^{sgs} = \frac{4}{3}\overline{\mu}\left(\widetilde{U_{k,k}^2} - \widetilde{U}_{k,k}^2\right), \end{cases} \tag{19}$$

where $\omega_i = \epsilon_{ijk}U_{k,j}$ is the vorticity and $\tilde{\omega}_i = \epsilon_{ijk}\widetilde{U}_{k,j}$ the filtered one with the permutation symbol ϵ_{ijk}. Comparing the governing equation of ρK_{utke} in Eq. (13) with the exact $\overline{\rho}K_{sgs}$ equation in Eq. (18), it is seen that the source term S_t in Eq. (13) is the net effect of SGS production term, SGS dissipation term and the SGS pressure-dilation transfer as

$$S_t \equiv P_{sgs} - D_{sgs} + \Pi_{sgs}. \tag{20}$$

Consequently, the current DtrKM in Eq. (4) provides an mesoscopic understanding in transport equation of the compressible SGS turbulence kinetic energy K_{sgs} in Eq. (18). The non-trivial quantity K_{utke} is proposed for modeling the unresolved turbulence structures, and the governing equation of K_{utke} is responsible for the evolution of unresolved turbulent process. This macroscopic description is consistent with the projection of DtrKM, namely, the double-relaxation kinetic model can be regarded as the mesoscopic understanding of one-equation SGS K_{sgs} model. We stress that the K_{utke} on unresolved grids will be regarded by default as SGS turbulence kinetic energy K_{sgs} on filtered grids. Especially, in the following modeling and simulations, the grid filter width is adopted as the effective grid length of control volume (see Sections 4.1 and 4.2) in the finite-volume numerical scheme, so K_{sgs} can be treated as K_{utke} by default. Similarly, the SGS variables are treated equivalently as unresolved variables without special statement.

As presented in Eq. (14), the connection between eddy viscosity μ_t and turbulent relaxation time τ_t is given by $\tau_t = \mu_t/p$. τ_t can be explained as the relaxation time for the turbulent eddies [27]. The larger turbulent relaxation time originates from the unresolved turbulence process, i.e., eddies transport and collision on unresolved grids. Following the seminal modeling strategy [17, 19], turbulent relaxation time τ_t and SGS stress τ_{ij}^{sgs} can be modeled as

$$\tau_t = \frac{C_s\overline{\Delta}\overline{\rho}K_{utke}^{\frac{1}{2}}}{p}, \tag{21}$$

$$\tau_{ij}^{sgs} = -2C_s\overline{\Delta}\overline{\rho}K_{utke}^{\frac{1}{2}}\widetilde{S}_{ij}^{*} + \frac{2}{3}\overline{\rho}K_{utke}\delta_{ij}, \tag{22}$$

where C_s is the model coefficient, $\overline{\Delta}$ the grid filter width, $\widetilde{S}_{ij}^{*} = \widetilde{S}_{ij} - \widetilde{S}_{kk}\delta_{ij}/3$ the traceless tensor of $\widetilde{S}_{ij}$. When correcting the total energy transport to recover the realistic turbulent Prandtl number Pr_t, the dynamic Prandtl number Pr_t can be modeled as

$$q_j = -C_s\overline{\Delta}\overline{\rho}K_{utke}^{\frac{1}{2}}\tilde{T}_{,j}/Pr_t. \tag{23}$$

As shown in Eq. (21), with the aid of essential gradient-type assumption, turbulent relaxation time τ_t has been closed in DtrKM. After modeling the SGS stress τ_{ij}^{sgs}, the SGS production term in source term in Eq. (20) is modeled correspondingly. For the left unknowns in source term S_t, the models of SGS dissipation rate and SGS pressure-dilation transfer read [19]

$$\epsilon_s^{sgs} = \frac{C_{\epsilon s}\overline{\rho}K_{utke}^{\frac{3}{2}}}{\overline{\Delta}}, \tag{24}$$

$$\epsilon_d^{sgs} = \frac{C_{\epsilon d}\overline{\rho}Ma_k^2K_{utke}^{\frac{3}{2}}}{\overline{\Delta}}, \tag{25}$$

$$\Pi_{sgs} = C_\Pi\overline{\Delta}^2\overline{p_{,j}}(\widetilde{U}_k)_{j,k}, \tag{26}$$

where $Ma_k^2 = 2K_{utke}/(\gamma RT)$ is the unresolved TKE Mach number. In terms of determining the unknown model coefficients, the current paper follows the standard dynamic approach [9, 10, 19]. In Eqs. (21) - (26), model coefficients C_s, C_Π and Pr_t can be dynamically computed through Germano identity [9, 10]. Additionally, $C_{\epsilon s}$ and $C_{\epsilon d}$ can be obtained by analogy with the relationship between the grid-filter-level SGS stress and the resolved stress across the test filter level [19, 49]. The detailed derivation of all dynamic model coefficients and necessary remarks are presented in Appendix 2.

The SGS concept from NS framework is highly appreciated, which provides the closure of the unknown terms among Eqs. (10)-(13) through the comparison with Eq. (18). Turbulent relaxation time τ_t and source term S_t have been modeled on the basis of Eqs. (20)-(26) with essential gradient-type assumption and standard dynamic approaches. In the subsequent section, instead of solving Eqs. (10)-(13) with the

traditional finite-volume hydrodynamic solver, the DtrKM in Eq. (4) is solved directly with the flux function provided by the time-dependent integral solution in the spirit of well-established gas-kinetic scheme [23, 24].

3 High-accuracy gas-kinetic scheme for DtrKM

For compressible turbulence modeling and simulation, besides constructing the physical models, the accurate and robust numerical scheme also plays the key role in handling the discontinuities and resolving the multi-scale structures on unresolved grids. In this section, to maintain the accurate and robust numerical performance of HGKS [44, 50, 51], the finite volume high-accuracy gas-kinetic scheme is proposed to solve DtrKM.

For finite volume method, the key procedure is updating the macroscopic flow variables inside each control volume through the numerical fluxes. Taking moments of the DtrKM in Eq. (4) and integrating with respect to control volume on unresolved grids, the finite volume scheme can be expressed as

$$\frac{\mathrm{d}(\boldsymbol{Q}_{ijk})}{\mathrm{d}t} = -\frac{1}{|\Omega_{ijk}|}\sum_{s=1}^{6}\mathbb{F}_s(t) + \boldsymbol{S}_{ijk}, \tag{27}$$

where $\boldsymbol{Q}_{ijk}$ is the cell averaged macroscopic variables in Eq. (6), $\boldsymbol{S}_{ijk}$ is the cell averaged source term in Eq. (7) with S_t modeled through Eqs. (20)-(26). The control volume $\Omega_{ijk} = [(x_1)_i - \Delta x_1/2, (x_1)_i + \Delta x_1/2]\cdot[(x_2)_j - \Delta x_2/2, (x_2)_j + \Delta x_2/2]\cdot[(x_3)_k - \Delta x_3/2, (x_3)_k + \Delta x_3/2]$, $|\Omega_{ijk}|$ is the volume of Ω_{ijk} and $\mathbb{F}_s(t)$ is the time-dependent numerical flux across the cell interface Σ_s. The numerical flux $\mathbb{F}_s(t)|_{x_1}$ in the x_1 direction (at cell interface $(x_1)_{i+1/2}$) is given as an example.

$$\begin{aligned}\mathbb{F}_s(t)|_{x_1} &= \iint_{\Sigma_s|_{x_1}} \boldsymbol{F}(\boldsymbol{Q})\cdot\boldsymbol{n}\mathrm{d}\sigma \\ &= \sum_{m,n=1}^{2}\omega_{mn}\int \boldsymbol{\psi}u_1 f(\boldsymbol{x}_{i+1/2,j_m,k_n}, t, \boldsymbol{u}, \xi, k_u)\mathrm{d}\Xi\Delta x_2\Delta x_3,\end{aligned} \tag{28}$$

where $\boldsymbol{n}$ is the outer normal direction. The Gaussian quadrature is used over the cell interface for Eq. (28), where ω_{mn} is the quadrature weight, $\boldsymbol{x}_{i+1/2,j_m,k_n} = [(x_1)_{i+1/2}, (x_2)_{j_m}, (x_3)_{k_n}]^T$, and $[(x_2)_{j_m}, (x_3)_{k_n}]$ is the quadrature point of cell interface $[(x_2)_j - \Delta x_2/2, (x_2)_j + \Delta x_2/2]\cdot[(x_3)_k - \Delta x_3/2, (x_3)_k + \Delta x_3/2]$. When constructing the numerical fluxes, the secondary relaxation term Q_s in Eq. (4) is not considered, and the effect of Q_s is taken into account as the source term in Eq. (27). The gas distribution function $f(\boldsymbol{x}_{i+1/2,j_m,k_n}, t, \boldsymbol{u}, \xi, k_u)$ in the local coordinate can be obtained by the integral solution of Eq. (4) as

$$\begin{aligned}f(\boldsymbol{x}_{i+1/2,j_m,k_n}, t, \boldsymbol{u}, \xi, k_u) =& \frac{1}{(\tau+\tau_t)}\int_0^t f^{eq}(\boldsymbol{x}', t', \boldsymbol{u}, \xi, k_u)e^{-(t-t')/(\tau+\tau_t)}\mathrm{d}t' \\ &+ e^{-t/(\tau+\tau_t)}f_0(-\boldsymbol{u}t, \xi, k_u),\end{aligned} \tag{29}$$

where $\boldsymbol{x}' = \boldsymbol{x}_{i+1/2,j_m,k_n} - \boldsymbol{u}(t-t')$ is the trajectory of molecules on unresolved grids, f_0 the initial gas distribution function, and f^{eq} the corresponding turbulence equilibrium state in the form of Eq. (5). Along the line of GKS [23, 50], for the multi-dimensional kinetic solver, f^{eq} and f_0 can be constructed as

$$f^{eq} = f_0^{eq}(1 + \overline{a}_1 x_1 + \overline{a}_2 x_2 + \overline{a}_3 x_3 + \overline{A} t), \tag{30}$$

and

$$f_0 = \begin{cases} f_l^{eq}\left[1 + \left(a_1^l x_1 + a_2^l x_2 + a_3^l x_3\right) - (\tau + \tau_t)\left(a_1^l u_1 + a_2^l u_2 + a_3^l u_3 + A_l\right)\right], & x \le 0, \\ f_r^{eq}\left[1 + \left(a_1^r x_1 + a_2^r x_2 + a_3^r x_3\right) - (\tau + \tau_t)\left(a_1^r u_1 + a_2^r u_2 + a_3^r u_3 + A_r\right)\right], & x > 0, \end{cases} \tag{31}$$

where f_l^{eq} and f_r^{eq} are the initial gas distribution functions on both sides of a cell interface Σ_s. f_0^{eq} is the initial turbulence equilibrium state located at the cell interface, which can be determined through the compatibility condition,

$$\int \boldsymbol{\psi} f_0^{eq} \mathrm{d}\Xi = \int_{u_1 > 0} \boldsymbol{\psi} f_l^{eq} \mathrm{d}\Xi + \int_{u_1 \le 0} \boldsymbol{\psi} f_r^{eq} \mathrm{d}\Xi. \tag{32}$$

Substituting f^{eq} (see Eq. (30)) and f_0 (see Eq. (31)) into Eq. (29), the time-dependent gas distribution function at the Gaussian point is evaluated as

$$\begin{aligned} f(\boldsymbol{x}_{i+1/2,j_m,k_n}, t, \boldsymbol{u}, \xi, k_u) &= (1 - e^{-t/(\tau+\tau_t)}) f_0^{eq} \\ &+ \left[(t + \tau + \tau_t)e^{-t\tau} - \tau\right](\overline{a}_1 u_1 + \overline{a}_2 u_2 + \overline{a}_3 u_3) f_0^{eq} \\ &+ \left[t - (\tau + \tau_t) + (\tau + \tau_t)e^{-t(\tau+\tau_t)}\right]\overline{A} f_0^{eq} \\ &+ e^{-t/(\tau+\tau_t)} f_l^{eq}\left[1 - (\tau + \tau_t + t)\left(a_1^l u_1 + a_2^l u_2 + a_3^l u_3\right) - (\tau + \tau_t)A_l\right] H(u_1) \\ &+ e^{-t/(\tau+\tau_t)} f_r^{eq}\left[1 - (\tau + \tau_t + t)\left(a_1^r u_1 + a_2^r u_2 + a_3^r u_3\right) - (\tau + \tau_t)A_r\right](1 - H(u_1)). \end{aligned} \tag{33}$$

With the relation of macroscopic variables and turbulence equilibrium distribution function f^{eq}, the spatial mesoscopic coefficients $\overline{a}_1$, $a_1^l, \cdots, a_3^l$, a_3^r and temporal mesoscopic coefficients $\overline{A}$, A_l, A_r in Eq. (33) can be determined and details are presented in Appendix 3. Equation (33) provides a gas evolution process from kinetic scale to hydrodynamic scale on unresolved grids, where both inviscid and viscous fluxes are recovered from a time-dependent and multi-dimensional gas distribution function at a cell interface. This flux function couples the inviscid and all dissipative terms [23, 50], and has advantages in comparison with traditional hydrodynamic solver in which the Riemann solver and central difference are used for the inviscid and viscous terms. For Prandtl number fix, both the laminar Prandtl number Pr and turbulent Prandtl number Pr_t should be taken into consideration. Total energy flux $\boldsymbol{F}(\rho E)$ in Eq. (28) should be modified as $\boldsymbol{F}^{new}(\rho E) = \boldsymbol{F}(\rho E) + \{(\mu Pr_t + \mu_t Pr)/[PrPr_t(\mu + \mu_t)] - 1\}q$, where the time-dependent heat flux can be evaluated precisely by $q = \int (u - U)\{[(u_i - U_i)^2 + \xi^2]/2 + k_u\} f d\Xi$.

The second-order accuracy in time can be achieved by one step integration, with the time-dependent kinetic flux in Eq. (33). To achieve high-order accuracy in space and time, the fifth-order WENO-Z spatial reconstruction [25] and two-stage fourth-order time discretization [44, 52] are implemented. The characteristic reconstruction is applied to improve the robustness for compressible flows with strong discontinuities (i.e., DCIT) [53]. The characteristic variables are defined as $Q_c = R^{-1}Q$, where $\boldsymbol{R}$ is the right eigenmatrix of Jacobian matrix at Gaussian quadrature point and details are given in Appendix 4. When dealing with compressible flows without strong discontinuities, such as TCPML, the linear WENO spatial reconstruction based on conservative variables is adopted. For source term in Eq. (27), the one-step forward Euler method is applied in two-stage updating process to

guarantee the robustness. Therefore, the finite volume high-accuracy gas-kinetic scheme has been constructed with the second-order kinetic flux, fifth-order WENO-Z reconstruction, two-stage fourth-order time discretization and one-step forward Euler method for source term. The current high-accuracy gas-kinetic scheme has been well implemented in the in-house platform for turbulence simulation [51], and the *a posteriori* tests on compressible turbulent flows will be presented in the following section.

4 *A posteriori* numerical tests

In this section, the decaying compressible isotropic turbulence [39, 40] and temporal compressible plane mixing layer [41–43] are regarded as cornerstones to assess DtrKM.

4.1 Decaying compressible isotropic turbulence

This section presents the numerical setup and the DtrKM for decaying compressible isotropic turbulence.

4.1.1 Numerical setup for DCIT

Decaying compressible isotropic turbulence [40] is the building-block case to demonstrate the performance of modeling on compressible turbulence. For the flow with discontinuities, we have

$$\tau + \tau_t = \frac{\mu + \mu_t}{p} + C_{num}\left|\frac{p_l - p_r}{p_l + p_r}\right|\mathrm{d}t, \tag{34}$$

where p is the pressure at the cell interface, p_l and p_r the pressure on the left and right sides of the cell interface. $\mathrm{d}t$ is the time step, and a fixed $C_{num} = 2.5$. The reason for including artificial dissipation through the additional term in the molecular relaxation time τ and the turbulent relaxation time τ_t is to improve the numerical stability with larger numerical dissipation. As the earlier remark states, the grid filter width is adopted as the grid length of control volume for DCIT, i.e., $\overline{\Delta} = \Delta x_1 = \Delta x_2 = \Delta x_3$ on equivalent spaced grids. Additionally, test filter width $\widehat{\overline{\Delta}}$ is set to twice the grid filter width $\overline{\Delta}$ when determining the dynamic model coefficients, namely $\widehat{\overline{\Delta}} = 2\overline{\Delta}$. DNS for DCIT has been well studied using HGKS systematically [20, 39]. In this section, following previous DNS set-up, LES on unresolved grids will be conducted directly.

In the computation, the initial Taylor microscale Reynolds number is $Re_{\lambda 0} = 72$ and the initial turbulent Mach number is fixed at $Ma_{t0} = 0.6$. The detailed initial conditions are set as in previous work [39], and the periodic boundary condition for six macroscopic variables is used. A three-dimensional solenoidal random initial velocity field can be generated by a specified spectrum as

$$E(\kappa) = A_0\kappa^4 \exp\left(-2\kappa^2/\kappa_0^2\right), \tag{35}$$

with the fixed $A_0 = 0.00013$ and $\kappa_0 = 8$. After generating the initial velocity field on 512^3 resolved grids, the filtered velocity fields can be obtained on unresolved grids, i.e., filtered flow fields on 128^3 grids. When filtering velocity field, the positive definite kernel of Box filter is adopted to guarantee the positive unresolved TKE [47]; thus the initial pointwise K_{utke0} on unresolved grids can be obtained as the initial condition for Eq.

(13). Table 1 shows the numerical parameters for DCIT of DNS and R_1, where κ_{max} is the maximum resolved wave number and η_0 is the Kolmogorov length scale. $\langle K_0 \rangle$ is the initial ensemble resolved TKE in which $\langle \cdot \rangle$ denotes the spatial average on the whole computational domain. Turbulence intensity I_0 denotes the ratio of initial ensemble unresolved $\langle K_{utke0} \rangle$ to the initial ensemble resolved TKE as $I_0 = \langle K_{utke0} \rangle / \langle K_0 \rangle$. Table 1 shows that the grid resolution meets the DNS criterion $\kappa_{max}\eta_0 \geq 2.71$ for DCIT [39]. Obviously, the grid resolution of R_1 is not adequate for DNS, which is regarded as compressible LES on unresolved grids.

The representative key statistical quantities as the resolved turbulence kinetic energy K, is given by

$$K = \frac{1}{2}\rho \boldsymbol{U}^2. \tag{36}$$

The ensemble budget of resolved K is computed, which can be described approximately by [16]

$$\frac{\mathrm{d}\langle K \rangle}{\mathrm{d}t} = -\langle \varepsilon \rangle + \langle pU_{k,k} \rangle, \tag{37}$$

$$\varepsilon = \varepsilon_s + \varepsilon_d, \tag{38}$$

where $\varepsilon_s = \mu \omega_i \omega_i$ is the resolved solenoidal dissipation rate, $\varepsilon_d = 4\mu U_{k,k}^2/3$ the resolved dilational dissipation rate without considering bulk viscosity, and $pU_{k,k}$ the resolved pressure-dilation transfer.

4.1.2 DtrKM for DCIT

Figure 2 shows the time history of dynamic coefficient C_s as in Eq. (21) for turbulent relaxation time τ_t and normalized ensemble $\langle K_{utke} \rangle / \langle K_{utke0} \rangle$. $\tau_{cit} = t/\tau_{to}$ is the normalized time and τ_{to} is the large-eddy-turnover time [39]. Firstly, model coefficient C_s is presented to validate the implementation of dynamic modeling approach in Appendix 2.2. The empirical model coefficient C_s is recommended as a fixed value 0.05 [7]. Figure 2a shows that the dynamic coefficient C_s in DtrKM fluctuates between [0.06, 0.12] for case R_1. The current dynamic approach shows that C_s reasonably depends on the grid resolution and the evolution of flow fields. In Fig. 2b, the normalized ensemble unresolved $\langle K_{utke} \rangle / \langle K_{utke0} \rangle$ increases approximately within $\tau_{cit} \leq 1.5$ and decreases consecutively, which behaves similarly to previous literature [19]. In Eq. (18), the SGS production term represents the inter-scale transfer associated with the interaction of resolved and unresolved scales. The SGS dissipation terms act as the sink of K_{utke} in source term S_t. The evolution of $\langle K_{utke} \rangle / \langle K_{utke0} \rangle$ implies that the ensemble forward resolved energy cascade dominates at the early stage, and then the SGS dissipation terms dominate. Figure 2b indicates that the intrinsic equilibrium assumption on K_{utke}, such as $\langle S_t \rangle \approx 0$ for

Table 1 Numerical parameters for DCIT

Case	Grid size	K_0	I_0	$\kappa_{max}\eta_0$
DNS	512^3	0.5055	0	3.6
R_1	128^3	0.4931	0.0151	0.90

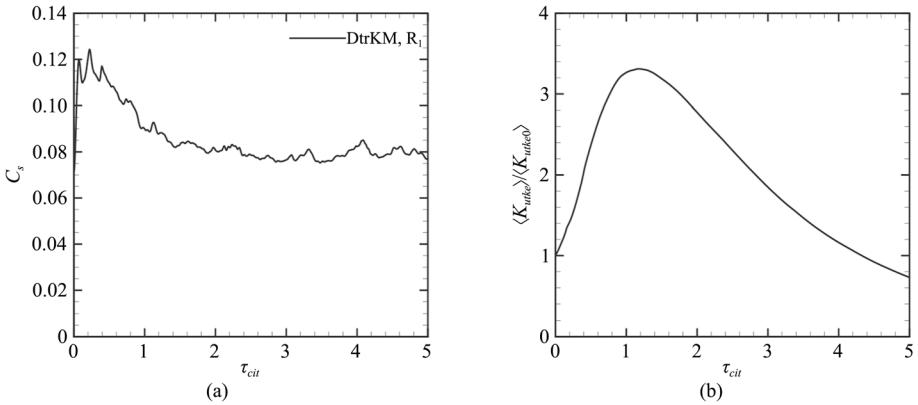

Fig. 2 Time history of **a** dynamic coefficient C_s and **b** normalized ensemble unresolved $\langle K_{utke}\rangle / \langle K_{utke0}\rangle$ for case R_1 with DtrKM

zero-equation eddy-viscosity LES models [3, 9, 10], is not valid, which confirms that the evolution of K_{utke} on unresolved grids is crucial for compressible LES modeling [7, 19].

Figure 3 shows the contours of unresolved K_{utke} and source term S_t at $\tau_{cit} = 0.5$ for case R_1. Figure 3a illustrates the contour of unresolved K_{utke}, and Fig. 3b confirms the ensemble positive source term S_t, which accounts for the increase of unresolved K_{utke} in Fig. 2b.

Figure 4 shows the key resolved statistical quantities in Eqs. (36)-(38) for case R_1. It is observed that the key statistical quantities of DtrKM are comparable with those from the widely-used DSM [10]. DSM is dealt with the equilibrium time-relaxation framework [30], which is also implemented in the in-house DNS code [51] with modifying the τ to $\tau + \tau_t$ on unresolved grids. Among these three compressible LES models, the heat flux is not modified, namely, $Pr = 1$ and $Pr_t = 1$ are treated fairly on all simulations. For density-weighted DSM, the eddy viscosity is determined as $\mu_t = C_{dsm}\overline{\Delta}^2\overline{\rho}|\widetilde{S}|$, and the dynamic coefficient C_{dsm} is computed through the dynamic technique presented in Appendix 2.1. The dynamic coefficient C_{dsm} in density-weighted DSM evolves between [0.016, 0.025] for case R_1. In conclusion, the performance of key statistical turbulent quantities shows that the current DtrKM is comparable with the widely-used DSM.

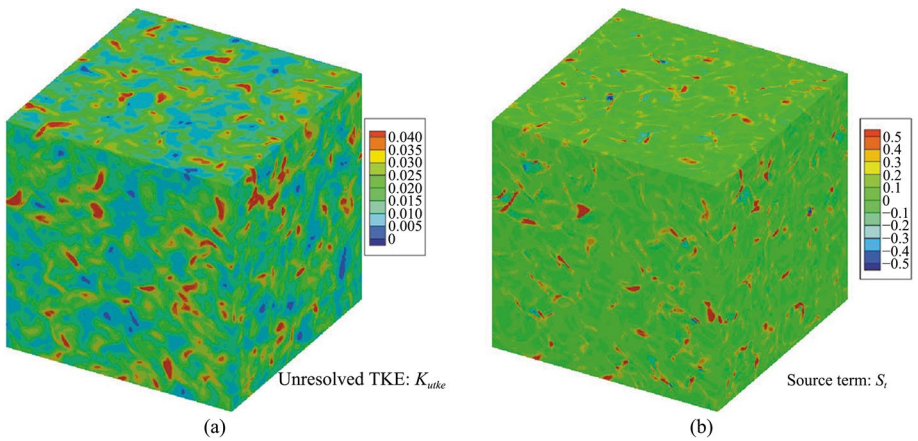

Fig. 3 Three-dimensional contours of **a** unresolved K_{utke} and **b** source term S_t at $\tau_{cit} = 0.5$ for case R_1 with DtrKM

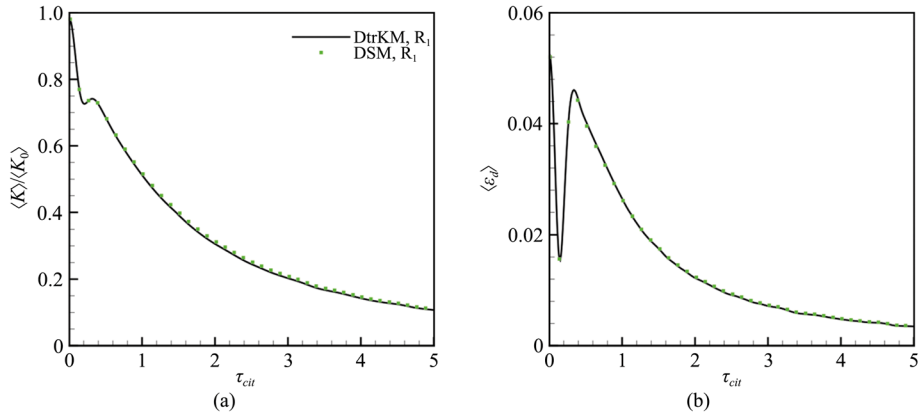

Fig. 4 Time history of **a** normalized ensemble resolved turbulence kinetic energy $\langle K\rangle/\langle K_0\rangle$ and **b** ensemble resolved dilational dissipation rate $\langle\varepsilon_d\rangle$ for case R_1

4.2 Temporal compressible plane mixing layer

This section first presents the numerical setup. The DNS is implemented to provide the coarse-grained initial flow fields for the subsequent DtrKM for a temporally compressible plane mixing layer.

4.2.1 Numerical setup for TCPML

For temporal compressible plane mixing layer [41–43], practical simulations on unresolved grids are conducted to further assess the performance of DtrKM and the high-accuracy gas-kinetic scheme (see Section 3). For the flow without strong discontinuities, the collision time is given by

$$\tau + \tau_t = \frac{\mu + \mu_t}{p}. \tag{39}$$

For TCPML, the grid filter width is adopted as the effective grid length of control volume, i.e., $\overline{\Delta} = (\Delta x_1 \times \Delta x_2 \times \Delta x_3)^{1/3}$. Test filter width $\widehat{\overline{\Delta}}$ still keeps to twice the grid filter width $\overline{\Delta}$ in determining the dynamic model coefficients, namely $\widehat{\overline{\Delta}} = 2\overline{\Delta}$. In this section, DNS in TCPML will be validated firstly. Then, LES studies restart from the filtered DNS solution on unresolved grids.

TCPML is initialized by a hyperbolic tangent profile for the streamwise velocity [54] as

$$\begin{cases} U_1 = \frac{1}{2}\Delta U \tanh\left(\frac{-x_2}{2\delta_{\theta 0}}\right), \\ U_2 = 0, \\ U_3 = 0, \end{cases} \tag{40}$$

where $\Delta U = U_{lo} - U_{up}$, and initial momentum thickness $\delta_{\theta 0} = 1$ is adopted. As Eq. (40) presents, two equal and opposite streamwise velocities are simulated as $-U_{up} = U_{lo} = 1$. With the unity Prandtl number, the Crocco-Busemann relation [55] gives the initial temperature profile as

$$\frac{T}{T_\infty} = 1 + Ma_c^2 \frac{\gamma - 1}{2}\left(1 - U_1^2\right). \tag{41}$$

The initial density is set to a uniform value ρ_∞. The convective Mach number $Ma_c = 0.75$ and initial vorticity thickness-based Reynolds number $Re_{\omega 0} = 640$ are simulated as

$$Ma_c = \frac{\Delta U}{2\sqrt{\gamma R T_\infty}}, \tag{42}$$

$$Re_{\omega 0} = \frac{\rho_\infty \Delta U \delta_{\omega 0}}{\mu_\infty}, \tag{43}$$

where μ_∞ is the reference viscosity corresponding to reference temperature T_∞, and viscosity is determined by power law as $\mu(T) = \mu_\infty (T/T_\infty)^{0.67}$ [41]. With the uniform initial density, initial vorticity thickness can be estimated as $\delta_{\omega 0} = \Delta U / |\partial U_1 / \partial x_2|_{max}$, in which the maximum of denominator is reached in the centre plane. $|\cdot|$ represents the absolute value. The momentum thickness δ_θ is defined as

$$\delta_\theta = \frac{1}{\rho_\infty (\Delta U)^2} \int_{-\infty}^{\infty} [\langle \rho U_1(x_2) \rangle - \langle \rho U_{lo} \rangle][\langle \rho U_{up} \rangle - \langle \rho U_1(x_2) \rangle] \mathrm{d}x_2, \tag{44}$$

where $\langle \bullet \rangle$ represents the plane average along the streamwise and spanwise directions, and $\delta_{\omega 0} \approx 4\delta_{\theta 0}$ is obtained in the finite transverse domain $[-L_1/2, L_1/2]$. For TCPML, the turbulent stress tensor R_{ij} and anisotropy stress tensor b_{ij} read

$$b_{ij} = \frac{R_{ij} - \frac{2}{3} K_R \delta_{ij}}{2K_R}, \tag{45}$$

$$R_{ij} = \frac{\left\langle \rho U_i^{'} U_j^{'} \right\rangle}{\langle \rho \rangle}, \tag{46}$$

where $U_i^{'} = U_i - \langle \rho U_i \rangle / \langle \rho \rangle$, K_R the so-called resolved turbulence kinetic energy as $K_R = R_{ii}/2$. Anisotropy stress tensor b_{ij} is an important characteristic of turbulence, especially for advanced turbulence closures [43]. In the following statistical process, R_{ij} is integrated across mixing layer within $[-\delta_\omega(\tau_{ml}), \delta_\omega(\tau_{ml})]$, while b_{ij} is integrated within $[-4\delta_\theta(\tau_{ml}), 4\delta_\theta(\tau_{ml})]$ with normalized time $\tau_{ml} = \Delta U t / \delta_{\theta 0}$. To accelerate the transition process, the initial condition is specified by adding a random number to density, temperature, transverse and spanwise velocities at each mesh point [41], i.e., $\rho_p = \rho_\infty + A_{s1} r_d e^{-x_2/(2\delta_{\theta 0})^2}$. r_d is a random number uniformly distributed between $[-0.5, 0.5]$ and the amplitude $A_{s1} = 0.2$. In terms of streamwise velocity, besides the random number, the artificial sinusoidal-type perturbation has been added as

$$U_{1p} = U_1 + U_1 [A_{s1} + A_{s2} \sin(\gamma_{s1} x_2)(B_{s1} + B_{s2})] r_d e^{-x_2/(2\delta_{\theta 0})^2}, \tag{47}$$

where $A_{s2} = 0.6$, $\gamma_{s1} = 0.25$, and $B_{s1} = A_{s3}[\cos(\gamma_{s2} x_1) + \cos(2\gamma_{s2} x_1) + \cos(4\gamma_{s2} x_1)]$, $B_{s2} = A_{s4}[\cos(\gamma_{s2} x_1)\cos(\gamma_{s2} x_3) + \cos(2\gamma_{s2} x_1)\cos(2\gamma_{s2} x_3) + \cos(4\gamma_{s2} x_1)\cos(4\gamma_{s2} x_3)$ with $A_{s3} = 0.2$, $A_{s4} = 0.4$ and $\gamma_{s2} = 0.235$. The initial condition for primitive variables $(\rho_p, U_{1p}, U_{2p}, U_{3p}, T_p)^T$ can be obtained for DNS. The computational domain is discretized uniformly in three directions. Boundary conditions in the homogeneous

streamwise and spanwise directions are periodic. In the transverse direction, the non-reflective boundary condition of conservative variables is given according to one-dimensional Riemann invariants [56], whereas the outlet boundaries are used for the unresolved K_{utke} (see Eq. (13)).

4.2.2 DNS for TCPML

Table 2 shows the numerical parameters for TCPML. Ref_1 was simulated by high-order finite difference method [43] with a smaller $Ma_c = 0.70$ and Ref_2 was simulated by WENO-enhanced GKS [54]. The size effect of computational domain and grid convergence have been well studied in Ref_2. Compared with the WENO-enhanced GKS [38], the current in-house code is equipped with the genuine spatial-temporal HGKS [44, 51]. Table 2 shows that the same computational domain and much finer grids are used by the current HGKS, which definitely guarantee the resolution of DNS. Figure 5 shows the contours of the magnitude of vorticity $\|\omega_{mg}\| = \sqrt{2\omega_i\omega_i}$ at $\tau_{ml} = 400$ and $\tau_{ml} = 1400$. Against the performance of $\|\omega_{mg}\|$ at transitional stage ($\tau_{ml} = 400$, see Fig. 5a), the magnitude of vorticity not only enlarges thicker but also behaves more intermittently at the self-similarity stage ($\tau_{ml} = 1400$, see Fig. 5b).

In Table 3, the normalized growth rate $\dot{\delta}_\theta/\dot{\delta}_{inc} = 0.589$ agrees well with that in Ref_2 [54], and is reasonably smaller than that of Ref_1 (smaller $Ma_c = 0.70$ corresponding to larger normalized momentum thickness) [43]. It is well known that compressibility suppresses the mixing layer growth rate $\dot{\delta}_\theta = \mathrm{d}\delta_\theta/\mathrm{d}\tau_{ml}$. Incompressible growth rate $\dot{\delta}_{inc} = 0.016$ is chosen for the hyperbolic tangent profile in Eq. (40). Growth rate in this paper is computed by the least-square method within $\tau_{ml} \in [1000, 1300]$ as shown in Fig. 6a. Table 3 also presents the vorticity thickness-based Reynolds number Re_ω and the

Table 2 Numerical parameters for TCPML

Case	$L_1 \times L_2 \times L_3$	$N_1 \times N_2 \times N_3$	Ma_c	$Re_{\omega 0}$
Ref_1	$172\delta_{\theta 0} \times 129\delta_{\theta 0} \times 86\delta_{\theta 0}$	256 × 192 × 128	0.70	640
Ref_2	$314\delta_{\theta 0} \times 157\delta_{\theta 0} \times 78.5\delta_{\theta 0}$	512 × 256 × 128	0.75	640
DNS	$314\delta_{\theta 0} \times 157\delta_{\theta 0} \times 78.5\delta_{\theta 0}$	576 × 384 × 192	0.75	640
M_1	$314\delta_{\theta 0} \times 157\delta_{\theta 0} \times 78.5\delta_{\theta 0}$	144 × 96 × 48	0.75	640

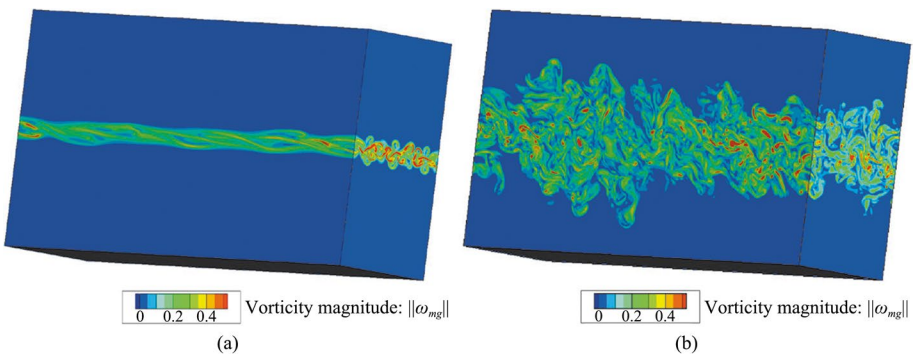

Fig. 5 Contours in magnitude of vorticity at **a** $\tau_{ml} = 400$ and **b** $\tau_{ml} = 1400$ for DNS

Table 3 Key quantities for DNS in TCPML at $\tau_{ml} = 1400$

Case	$\dot{\delta}_\theta / \dot{\delta}_{inc}$	Re_ω	Ma_t	(b_{11}, b_{12}, b_{22})
Ref_1	0.675	7790	-	(0.15, 0.15, −0.10)
Ref_2	0.589	8160	0.30	(0.13, 0.13, −0.12)
DNS	0.588	8052	0.28	(0.14, 0.16, −0.07)

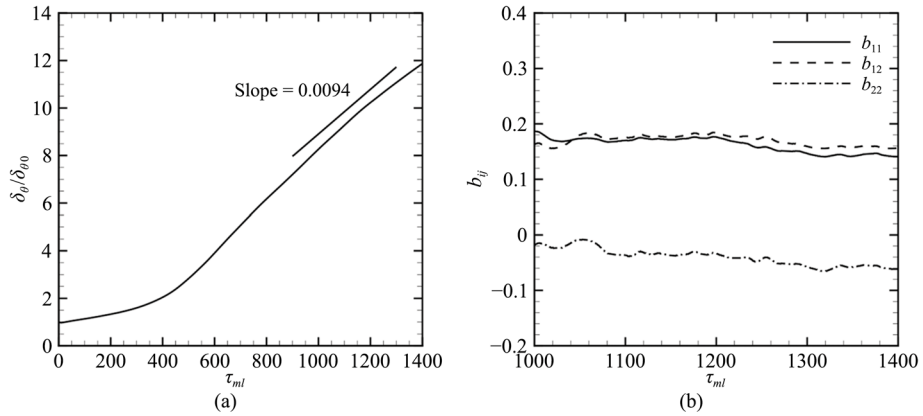

Fig. 6 Time history of **a** normalized momentum thickness $\delta_\theta / \delta_{\theta 0}$ and **b** evolution of anisotropy stress tensor b_{ij} for DNS

turbulent Mach number Ma_t at $\tau_{ml} = 1400$. Here, turbulent Mach number is defined as $Ma_t^2 = 2K_R/(\gamma R T_\infty)$. Table 3 shows that Re_ω and Ma_t at the center plane are in good agreement for all cases. (In Ref_1 and Ref_2, the ending of the simulation may be $\tau_{ml} = 600$). Figure 6b shows the time history of anisotropy stress tensor b_{ij} in Eq. (45). We observe the well-matched quasi-stationary profiles during the self-similarity stage. Table 3 shows the components of anisotropy stress tensor (b_{11}, b_{12}, b_{22}) at $\tau_{ml} = 1400$. The large deviation in b_{22} can be attributed to the differences in setting up the initial perturbation field [54]. Overall, the current DNS results agree well with refereed numerical simulations.

4.2.3 DtrKM for TCPML

With the high-fidelity flow fields from DNS, M_1 with DtrKM and DSM is conducted on unresolved grids. Figure 7a shows the initial pointwise unresolved TKE. The initial unresolved

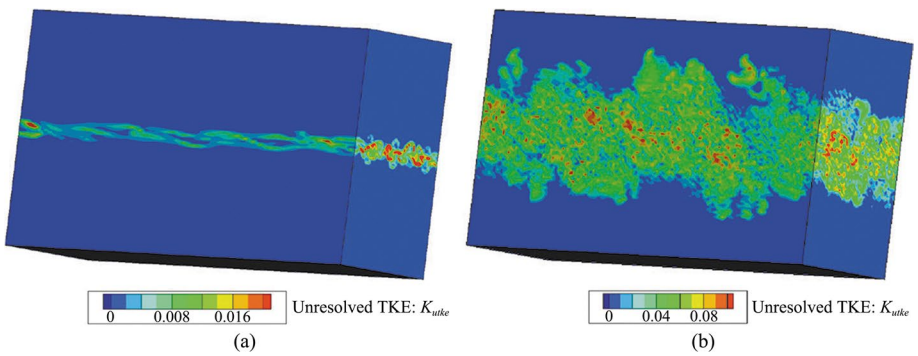

Fig. 7 Contours of unresolved K_{utke} at **a** $\tau_{ml} = 400$ and **b** $\tau_{ml} = 1400$ for case M_1 with DtrKM

K_{utke} is in a small magnitude and restricted in a narrow region. From transitional stage to self-similarity stage (at $\tau_{ml} = 1400$), Fig. 7b shows that the magnitude of unresolved K_{utke} increases obviously, and entrains to a much wider region similar to that in Fig. 5b. Again, the intrinsic equilibrium assumption on K_{utke}, such as $\langle S_t \rangle \approx 0$ for zero-equation eddy-viscosity LES models [3, 9, 10], may not hold. Box filter is used to generate the initial (restarted) six-variable flow field (see Eqs. (10)-(13)) from the DNS solution at $\tau_{ml} = 400$, i.e., 4^3 resolved grids are coarsen to 1 unresolved grid. Table 2 shows that M_1 with DtrKM and DSM is conducted on unresolved uniform grids $144 \times 96 \times 48$. The same computational domain and boundary conditions are applied as in the DNS. When implementing DtrKM, the minimum unresolved TKE is set as $\langle K_{utke0} \rangle / 10000$, where the initial ensemble unresolved $\langle K_{utke0} \rangle = 0.00058$.

Figure 8a shows the time history of ensemble unresolved $\langle K_{utke} \rangle$ from DtrKM and ensemble resolved kinetic energy $\langle K \rangle$. The ensemble unresolved TKE from DtrKM increases, while the ensemble resolved kinetic energy $\langle K \rangle$ decreases in the dissipative system. Figure 8b also shows the evolution of normalized momentum thickness $\delta_\theta / \delta_{\theta 0}$. Figure 8 shows that the performance of statistical quantities from DtrKM agrees well with that from DSM. In Table 4, the normalized growth rate $\dot{\delta}_\theta / \dot{\delta}_{inc} = 0.611$ from DtrKM agrees well with that from DSM, slightly larger than that of DNS.

Table 4 shows the vorticity thickness-based Reynolds number Re_ω, and the turbulent Mach number Ma_t from LES at $\tau_{ml} = 1400$ at the center plane. The vorticity thickness-based Reynolds numbers Re_ω based on two LES models are larger than that of DNS, where the turbulent Mach number Ma_t from LES agrees well with that of DNS. Components of anisotropy stress tensor at $\tau_{ml} = 1400$ agree well with each other in b_{11} and b_{12} (see Eq. (45)). Figure 9 presents the profiles of normalized turbulent stress $(R_{11})^{1/2}/\Delta U$, $(R_{22})^{1/2}/\Delta U$, $(R_{33})^{1/2}/\Delta U$, and $(R_{12})^{1/2}/\Delta U$ (see Eq. (46)). The normalized turbulent stress from two LES models shows quite small deviations. In TCPML, the performance

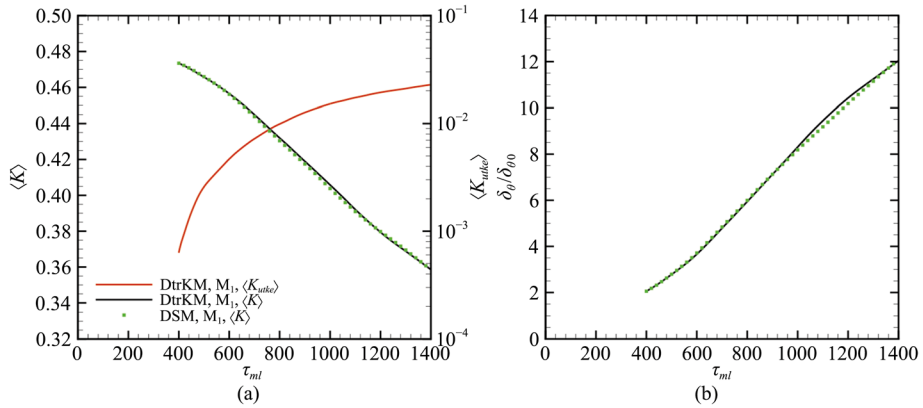

Fig. 8 Time history of **a** ensemble unresolved $\langle K_{utke} \rangle$ (only from DtrKM) and ensemble resolved kinetic energy $\langle K \rangle$, and **b** normalized momentum thickness $\delta_\theta / \delta_{\theta 0}$ for case M_1

Table 4 Key quantities for LES in TCPML at $\tau_{ml} = 1400$

Case M_1	$\dot{\delta}_\theta / \dot{\delta}_{inc}$	Re_ω	Ma_t	(b_{11}, b_{12}, b_{22})
DtrKM	0.611	11912	0.27	(0.13, 0.16, −0.08)
DSM	0.619	11814	0.30	(0.15, 0.15, −0.08)

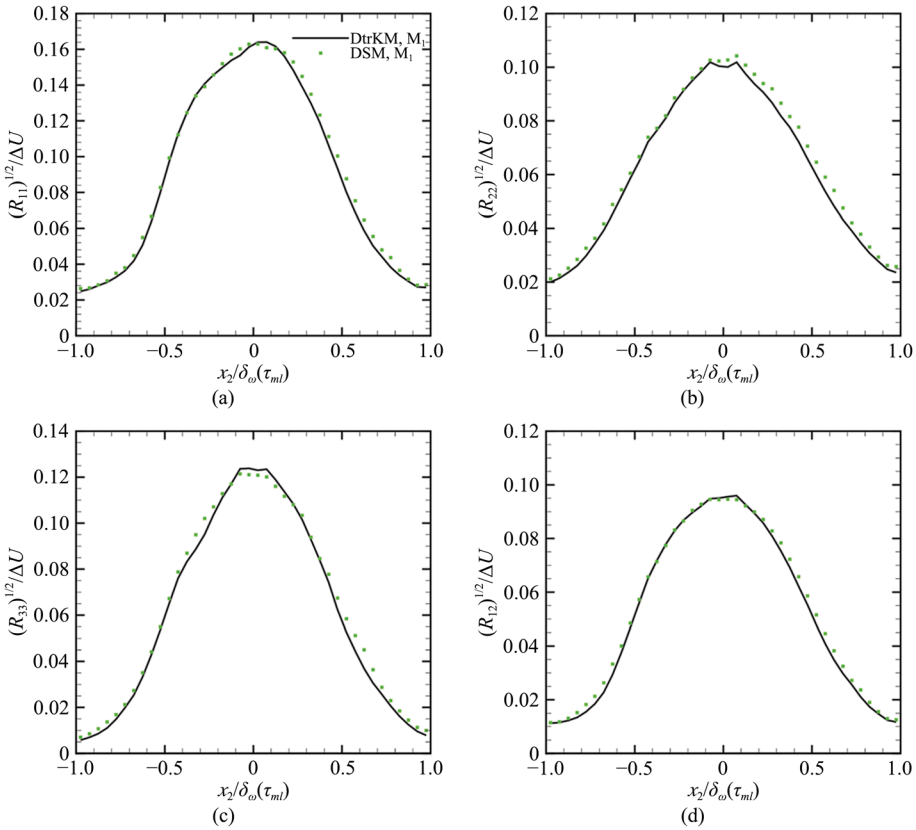

Fig. 9 Profiles of normalized turbulent stress **a** $(R_{11})^{1/2}/\Delta U$, **b** $(R_{22})^{1/2}/\Delta U$, **c** $(R_{33})^{1/2}/\Delta U$ and **d** $(R_{12})^{1/2}/\Delta U$ for case M_1

of key turbulent quantities up to second-order statistics confirms that the current DtrKM is comparable with the widely-used DSM.

5 Conclusion and discussion

We propose the double time-relaxation kinetic model for compressible turbulence modeling for the first time. The key idea is to construct the non-trivial turbulent quantities and their corresponding dynamic evolution quantitatively on unresolved grids. Within the double time-relaxation framework, DtrKM is constructed in the form of a modified BGK model on unresolved grids. Based on the first-order Chapman-Enskog expansion, DtrKM connects with the six-variable macroscopic governing equations. Phenomenologically, the unknown turbulent relaxation time and source term in DtrKM are determined by gradient-type assumption and dynamic modeling approach. Therefore, the double time-relaxation kinetic model provides a profound mesoscopic understanding for transport equation of the compressible SGS turbulence kinetic energy. To solve the DtrKM accurately and robustly, a finite volume high-accuracy gas-kinetic scheme is developed in the spirit of the well-established gas-kinetic scheme. DCIT and TCPML are simulated as benchmarks to evaluate the current double time-relaxation kinetic model and high-accuracy gas-kinetic scheme. The performance of key statistical turbulent quantities up to second-order statistics confirms that the current DtrKM is comparable

with the widely-used DSM. The present work not only points to an alternative way for compressible turbulence modeling on unresolved grids, but also opens great possibilities to simulate multi-scale flow physics within the double time-relaxation framework.

In terms of the current high-accuracy gas-kinetic scheme for DtrKM, it is natural to inherit the numerical strength from the well-developed HGKS, i.e., the robust performance from the subsonic to hypersonic viscous heat conducting flows [50]. To explore the benefits, DtrKM will be further implemented for more practical highly compressible turbulent flows, such as compressible wall-bounded turbulent flows and shock-boundary layer interaction [57, 58]. Compared with incompressible turbulence, compressible turbulent flows are more complex due to the non-linear coupling of velocity, density, and pressure fields. Consequently, compressible LES models are much more difficult to construct than the incompressible ones. Being of scientific interest, the optimal physical distribution of K_{utke} and the direct modeling of the source term in Eq. (8) on unresolved grids, still require continuous effort in understanding the unresolved properties of turbulence. To that extent, a complete time-relaxation compressible turbulence modeling without any ad-hoc technique from macroscopic turbulence models may be achieved. The turbulent relaxation time τ_t can be far larger than the molecular relaxation time τ on unresolved grids. The formal first-order Chapman-Enskog expansion in Appendix 1 may not be such solid. If DtrKM can be solved by a multi-scale kinetic solver, such as UGKS [46], the multi-scale fluxes can improve its performance and overcome the limitation of Chapman-Enskog expansion correspondingly. These challenging topics deserve to be explored in subsequent studies. Additionally, detailed comparisons on accuracy, efficiency, and robustness between the current DtrKM and classical SGS models with solving NS equations are supposed to be studied in the future.

Appendix 1 Connection between double time-relaxation kinetic model and macro governing equations

This appendix provides the details for the derivation of corresponding macroscopic governing equations on unresolved grids based on the DtrKM. Derivation of the Euler equations and the NS equations from the BGK model can be found in Appendix 2 [23]. Similar to molecular relaxation time $\tau = \epsilon\hat{\tau}$ in refereed derivation, the turbulent relaxation time is rewritten as $\tau_t = \epsilon\hat{\tau}_t$, in which ϵ is a small dimensionless quantity. Suppose that f^{eq} has a Taylor series expansion about point $(\boldsymbol{x}, t)$. Since τ and τ_t depend on the local thermodynamic variables and unresolved K_{utke}, and these depend on the moments of f^{eq}, we may assume that τ and τ_t are consequently $\hat{\tau}$ and $\hat{\tau}_t$, and can be expanded about the point $(\boldsymbol{x}, t)$. Now, consider the formal solution of the DtrKM for $f(\boldsymbol{x}, t, \boldsymbol{u}, \xi, k_u)$, supposing that f^{eq} is known, it can be shown that $f(\boldsymbol{x}, t, \boldsymbol{u}, \xi, k_u)$ has an expansion in powers of ϵ.

We derive the terms in this expansion from the formal solution of $f(\boldsymbol{x}, t, \boldsymbol{u}, \xi, k_u)$, by putting the power expansion $f = f_0 + \epsilon f_1 + \epsilon^2 f_2 + \cdots$, and $(\tau + \tau_t) = \epsilon(\hat{\tau} + \hat{\tau}_t)$ into the DtrKM directly. Let $D_{\boldsymbol{u}} = \partial/\partial t + u_i \partial/\partial x_i$, and write the DtrKM as $\epsilon(\hat{\tau} + \hat{\tau}_t) D_{\boldsymbol{u}} f + f - f^{eq} = 0$, with handling the source term Q_s in Eq. (4) separately. An expansion of this equation in powers of ϵ yields

$$f = g - \epsilon(\hat{\tau} + \hat{\tau}_t)D_{\boldsymbol{u}}f^{eq} + \epsilon^2(\hat{\tau} + \hat{\tau}_t)D_{\boldsymbol{u}}((\hat{\tau} + \hat{\tau}_t)D_{\boldsymbol{u}}f^{eq}) + \cdots. \tag{48}$$

According to the compatibility condition, after dividing by $\epsilon(\hat{\tau} + \hat{\tau}_t)$, we obtain

$$\int \boldsymbol{\psi} D_{\boldsymbol{u}}f^{eq}\mathrm{d}\Xi = \epsilon \int \boldsymbol{\psi} D_{\boldsymbol{u}}[(\hat{\tau} + \hat{\tau}_t)D_{\boldsymbol{u}}f^{eq}]\mathrm{d}\Xi + \mathcal{O}(\epsilon^2), \tag{49}$$

where $\boldsymbol{\psi} = \left(1, u_1, u_2, u_3, \frac{1}{2}\left(u_1^2 + u_2^2 + u_3^2 + \xi^2\right) + k_u, k_u\right)^T$, and $\mathrm{d}\Xi = \mathrm{d}u_1\mathrm{d}u_2\mathrm{d}u_3\mathrm{d}\xi\,\mathrm{d}k_u$. The integral on the left-hand-side $\mathcal{L}_\alpha$ and the right-hand-side $\mathcal{R}_\alpha$ of Eq. (49) can be defined as

$$\mathcal{L}_\alpha = \epsilon\mathcal{R}_\alpha + \mathcal{O}(\epsilon^2), \tag{50}$$

which shows that $\mathcal{L}_\alpha$ is at least $\mathcal{O}(\epsilon)$, obviously. Therefore, in reducing the $\mathcal{R}_\alpha$ on the right side of Eq. (50), which is already $\mathcal{O}(\epsilon)$, we can drop $\mathcal{O}(\epsilon)$ quantities and their derivatives. To simplify the notation, let

$$\langle\psi_\alpha(\cdot)\rangle \equiv \int \psi_\alpha f^{eq}\mathrm{d}\Xi, \quad \alpha = 1, 2, 3, 4, 5, 6, \tag{51}$$

where $\langle\psi_\alpha(\cdot)\rangle$ denotes the moments of f^{eq} on ψ_α, and ψ_α is the component of $\boldsymbol{\psi}$. Therefore, $\mathcal{L}_\alpha$ and $\mathcal{R}_\alpha$ are rewritten as

$$\begin{aligned} \mathcal{L}_\alpha =& \langle\psi_\alpha\rangle_{,t} + \langle\psi_\alpha u_l\rangle_{,l}, \\ \mathcal{R}_\alpha =& \{(\hat{\tau} + \hat{\tau}_t)[\langle\psi_\alpha u_k\rangle_{,t} + \langle\psi_\alpha u_k u_l\rangle_{,l}]\}_{,k} + \mathcal{O}(\epsilon), \end{aligned} \tag{52}$$

where k and l are subscripts of molecular velocity, taking from 1 to 3 for three-dimension derivation. The macroscopic governing equations in Euler-type and NS-type can be obtained by truncating Eq. (50) up to the order of $\mathcal{O}(1)$ and $\mathcal{O}(\epsilon)$, respectively. The Euler-type macroscopic equations can be derived straightforwardly by the Chapman-Enskog expansion up to zeroth order, which are used to simplify the derivation of NS-type equations. This appendix focuses on the NS-type macroscopic equations by the Chapman-Enskog expansion up to first order truncation of $\tau + \tau_t$.

1.1 Continuity equation

Continuity equation is derived straightforwardly as

$$\rho_{,t} + (\rho U_k)_{,k} = 0, \tag{53}$$

which can be used to simplify the momentum equations, the total energy equations, and the unresolved TKE equation.

1.2 Momentum equation

To simplify the time derivative of pressure in the momentum equations, we introduce the following procedure firstly. For total energy equation, the left side $\mathcal{L}_5$ of Eq. (50) can be grouped as

$$\begin{aligned}\mathcal{L}_5 =& \frac{1}{2}U_n^2[\rho_{,t} + (\rho U_k)_{,k}] + \rho U_n U_{n,t} + \rho U_k U_n U_{n,k} + U_k p_{,k} \\ &+ \frac{N+3}{2}[p_{,t} + U_k p_{,k}] + \frac{N+5}{2} p U_{k,k} + (\rho K_{utke})_{,t} + (\rho K_{utke} U_k)_{,k},\end{aligned} \tag{54}$$

where N is the total number of degrees of freedom in ξ. The first term is $U_n^2\mathcal{L}_1/2$, which is $\mathcal{O}(\epsilon^2)$, and the next three are $U_n\mathcal{L}_n$, and are therefore $\mathcal{O}(\epsilon)$. Then $\mathcal{L}_5$ can be rewritten as

$$\begin{aligned}\mathcal{L}_5 =& \frac{N+3}{2}[p_{,t} + U_k p_{,k}] + \frac{N+5}{2} p U_{k,k} + U_n\mathcal{L}_n \\ &+ (\rho K_{utke})_{,t} + (\rho K_{utke} U_k)_{,k} + \mathcal{O}(\epsilon^2).\end{aligned} \tag{55}$$

Based on the Chapman-Enskog expansion up to zeroth order, unresolved TKE equation $\mathcal{L}_6$ in Euler-type can be written as

$$\mathcal{L}_6 = (\rho K_{utke})_{,t} + (\rho K_{utke} U_k)_{,k} - S_t + \mathcal{O}(\epsilon), \tag{56}$$

which can be used to simplify the time derivative of $(\rho K_{utke})_{,t}$ in the following derivation. Combining Eqs. (55) and (56), we get

$$p_{,t} + U_k p_{,k} = -\frac{N+5}{N+3} p U_{k,k} - \frac{2S_t}{N+3} + \mathcal{O}(\epsilon), \tag{57}$$

which can be used to simplify the time derivative of pressure $p_{,t}$ in the following derivation.

For the right hand sides of the momentum equations in Eq. (50), considering $\mathcal{R}_j = [(\hat{\tau} + \hat{\tau}_t)F_{jk}]_{,k}$, we get

$$\begin{aligned}F_{jk} =& \langle u_j u_k\rangle_{,t} + \langle u_j u_k u_l\rangle_{,l} \\ =& U_j[(\rho U_k)_{,t} + [(\rho U_k U_l) + p\delta_{kl}]_{,l}] + \rho U_k U_{j,t} + (p\delta_{jk})_{,t} \\ &+ (\rho U_k U_l + p\delta_{kl})U_{j,l} + (U_l p\delta_{jk} + U_k p\delta_{jl})_{,l},\end{aligned} \tag{58}$$

where the fact that all odd moments in w_k vanish has been used. Here $w_k = u_k - U_k$ is the peculiar velocity. The term in square brackets multiplying U_j is $\mathcal{L}_k$, i.e., it is $\mathcal{O}(\epsilon)$, and can therefore be ignored. Then, after gathering terms with coefficients U_k and p, we have

$$F_{jk} = U_k[\rho U_{j,t} + \rho U_l U_{j,l} + p_{,j}] + p[U_{k,j} + U_{j,k} + U_{l,l}\delta_{jk}] + \delta_{jk}[p_{,t} + U_l p_{,l}] + \mathcal{O}(\epsilon). \tag{59}$$

The coefficient of U_k can be simplified by the following equation,

$$\mathcal{L}_i = \rho U_{i,t} + \rho U_k U_{i,k} + p_{,i} + \mathcal{O}(\epsilon^2), \tag{60}$$

where Eq. (60) is derived by multiplying the continuity equation by U_i and subtracting the result from $\mathcal{L}_i$ ($i = 2, 3, 4$). To eliminate $p_{,t}$ from the last term we use Eq. (57) for $\mathcal{L}_5$. Finally, decompose the tensor $U_{k,j}$ into its dilation and shear parts in the usual way, which gives

$$F_{jk} = p\left[U_{k,j} + U_{j,k} - \frac{2}{3}U_{l,l}\delta_{jk}\right] + \frac{2}{3}\frac{N}{(N+3)}pU_{l,l}\delta_{jk} - \frac{2S_t}{N+3}\delta_{jk} + \mathcal{O}(\epsilon). \tag{61}$$

The second term is due to bulk viscosity involving energy sharing between translational and internal degrees of freedom of the molecules [24, 59], and the last term results from the energy interaction between the resolved kinetic energy and the unresolved TKE.

1.3 Total energy equation

In analogy with the derivation of the NS total energy equation, we write $\mathcal{R}_5 = \{(\hat{\tau} + \hat{\tau}_t)N_k\}_{,k}$ with

$$N_k = \left\langle u_k\left(\frac{u_n^2+\xi^2}{2} + k_u\right)\right\rangle_{,t} + \langle u_k u_l\left(\frac{u_n^2+\xi^2}{2} + k_u\right)\rangle_{,l}, \tag{62}$$

where the k_u is the sample-space variable corresponding to unresolved K_{utke}. N_k can be decomposed into $N_k = N_k^{(1)} + N_k^{(2)}$, where

$$N_k^{(1)} = \left[U_k\left(\frac{u_n^2+\xi^2}{2} + k_u\right)\right]_{,t} + \left[U_k\left\langle u_l\left(\frac{u_n^2+\xi^2}{2} + k_u\right)\right\rangle\right]_{,l}, \tag{63}$$

and

$$N_k^{(2)} = \left\langle w_k\left(\frac{u_n^2+\xi^2}{2} + k_u\right)\right\rangle_{,t} + \left\langle w_k u_l\left(\frac{u_n^2+\xi^2}{2} + k_u\right)\right\rangle_{,l}. \tag{64}$$

For $N_k^{(1)}$, we have

$$\begin{aligned} N_k^{(1)} =& U_k\left[\left\langle\frac{u_n^2+\xi^2}{2} + k_u\right\rangle_{,t} + \left\langle u_l\left(\frac{u_n^2+\xi^2}{2} + k_u\right)\right\rangle_{,l}\right] \\ &+ \left[\frac{1}{2}\rho U_n^2 + \frac{N+3}{2}p + \rho K_{utke}\right]U_{k,t} + \left[U_l\left(\frac{1}{2}\rho U_n^2 + \frac{N+5}{2}p + \rho K_{utke}\right)\right]U_{k,l}. \end{aligned} \tag{65}$$

The coefficient of U_k in the equation above is $\mathcal{L}_5$, and therefore can be dropped, and the remaining terms can be rewritten as

$$N_k^{(1)} = \left[\frac{1}{2}\rho U_n^2 + \frac{N+3}{2}p + \rho K_{utke}\right]\left[U_{k,t} + U_l U_{k,l}\right] + pU_l U_{k,l} + \mathcal{O}(\epsilon). \tag{66}$$

After replacing $U_{k,t}$ according to Eq. (60), we get

$$N_k^{(1)} = -\left[\frac{1}{2}U_n^2 + \frac{N+3}{2}\frac{p}{\rho} + K_{utke}\right]p_{,k} + pU_l U_{k,l} + \mathcal{O}(\epsilon). \tag{67}$$

For $N_k^{(2)}$, remembering that odd moments in w_k vanish, we have

$$\begin{aligned} N_k^{(2)} =&\langle U_n w_n w_k\rangle_{,t} + \langle U_l U_n w_n w_k\rangle_{,l} \\ &+ \frac{1}{2}\left\langle U_n^2 w_k w_l\right\rangle_{,l} + \left\langle w_k w_l\left(\frac{w_n^2+\xi^2}{2}+k_u\right)\right\rangle_{,l} \\ =&(pU_k)_{,t} + (pU_kU_l)_{,l} + \frac{1}{2}(U_n^2 p)_{,k} + \frac{N+5}{2}\left(\frac{p^2}{\rho}\right)_{,k} + (pK_{utke})_{,k}. \end{aligned} \tag{68}$$

$N_k^{(2)}$ can be rewritten as

$$\begin{aligned} N_k^{(2)} =&p\left[U_{k,t} + U_l U_{k,l} + U_k U_{l,l} + U_l U_{l,k}\right] \\ &+ U_k\left(p_{,t} + U_l p_{,l}\right) + \frac{1}{2}U_n^2 p_{,k} + \frac{N+5}{2}\left(\frac{p^2}{\rho}\right)_{,k} + (pK_{utke})_{,k}. \end{aligned} \tag{69}$$

The $p_{,t}$ and $U_{k,t}$ can be replaced by Eqs. (57) and (60), respectively. Hence

$$\begin{aligned} N_k^{(2)} =&p\left[-\frac{p_{,k}}{\rho} + U_k U_{l,l} + U_l U_{l,k}\right] + U_k\left[-\frac{N+5}{N+3}pU_{l,l} - \frac{2S_t}{N+3}\right] \\ &+ \frac{1}{2}U_n^2 p_{,k} + \frac{N+5}{2}\left(\frac{p^2}{\rho}\right)_{,k} + (pK_{utke})_{,k} + \mathcal{O}(\epsilon). \end{aligned} \tag{70}$$

Finally, N_k can be obtained by summing $N_k^{(1)}$ and $N_k^{(2)}$ up

$$\begin{aligned} N_k =&p\left[U_l(U_{k,l} + U_{l,k}) - \frac{2}{N+3}U_k U_{l,l}\right] - U_k\frac{2S_t}{N+3} \\ &+ \frac{N+5}{2}p\left(\frac{p}{\rho}\right)_{,k} + (pK_{utke})_{,k} + \mathcal{O}(\epsilon). \end{aligned} \tag{71}$$

1.4 Unresolved turbulence kinetic energy equation

For unresolved K_{utke} equation, we write $\mathcal{R}_6 = \{(\hat{\tau}+\hat{\tau}_t)Z\}_{,k}$, where

$$\begin{aligned} Z =&\langle k u_k\rangle_{,t} + \langle k u_k u_l\rangle_{,l} \\ =&K_{utke}[(\rho U_k)_{,t} + (\rho U_k U_l + p\delta_{kl})_{,l}] + \rho U_k K_{utke,t} + K_{utke,l}[\rho U_k U_l + p\delta_{kl}]. \end{aligned} \tag{72}$$

The term in square brackets is $\mathcal{L}_k$, i.e., $\mathcal{O}(\epsilon)$, and can be dropped. Equation (56) subtracts the multiplication of the continuity equation (53) by K_{utke}, and we obtain

$$\mathcal{L}_6 = \rho K_{utke,t} + \rho U_l K_{utke,l} - S_t + \mathcal{O}(\epsilon^2). \tag{73}$$

Gathering terms with coefficients U_k and p, and replacing $K_{utke,t}$ through Eq. (73), we have

$$Z = U_k S_t + pK_{utke,k} + \mathcal{O}(\epsilon). \tag{74}$$

All time derivatives have now been removed from $\mathcal{R}_\alpha$, and the remaining steps in deriving corresponding macroscopic governing equations for DtrKM may be summarized briefly as

- Drop $\mathcal{O}(\epsilon^2)$ in Eq. (50),
- Combine ϵ and $\hat{\tau}+\hat{\tau}_t$ to recover $\tau+\tau_t=\epsilon(\hat{\tau}+\hat{\tau}_t)$,
- Define the molecular dynamic viscosity as $\mu=\tau p$, and the turbulent eddy viscosity is recovered by $\mu_t=\tau_t p$,
- Define the molecular thermal conductivity $\kappa=(N+5)\tau p/2$, and the turbulent thermal conductivity $\kappa_t=(N+5)\tau_t p/2$.

Finally, corresponding macroscopic governing equations for DtrKM can be rewritten as Eqs. (10)-(13) in Section 2.4.

Appendix 2 Dynamic approach to determine model coefficients

Model coefficients C_s, Pr_t, and C_Π can be dynamically computed through Germano identity [9, 11], which assumes the similarity of SGS quantities between the grid filter width $\overline{\Delta}$ and the test filter width $\widehat{\overline{\Delta}}$. In finite volume framework, explicit filter is not used, while the grid length of control volume itself acts as the grid filter width, and the projection process when updating the macroscopic variables can be regarded as the filtering process. For any term $\phi=\overline{\beta_1\beta_2}-\overline{\beta}_1\overline{\beta}_2$ on grid filter level, assuming that $\Phi=\widehat{\overline{\beta_1\beta_2}}-\widehat{\overline{\beta}}_1\widehat{\overline{\beta}}_2$ still holds on test filter level. Then, the resolved tensor (or vector/scalar) is defined as $L=\Phi-\widehat{\phi}$. Assume ϕ is modeled by the linear constitutive relationship $\phi=Cm$, where m is a function of the resolved quantities. At the test filter level, $\Phi=CM$, M takes a similar form to m but is a function of the test-filtered quantities. Plugging the linear model for Φ and ϕ, the Germano identity reads

$$L=\widehat{\overline{\beta}_1\overline{\beta}_2}-\widehat{\overline{\beta}}_1\widehat{\overline{\beta}}_2=C(M-\widehat{m}). \tag{75}$$

To avoid computational instability, C can be optimized by the least-square method [11].

2.1 Dynamic coefficient for density-weighted Smagorinsky model

For density-weighted DSM [10], the model coefficient C_{dsm} is determined by

$$\begin{cases} L_{ij}^*=-2C_{dsm}M_{ij}, \\ M_{ij}=\widehat{\overline{\Delta}}^2\widehat{\overline{\rho}}\widehat{\overline{S}}\widehat{\overline{S}}_{ij}^*-\overline{\Delta}^2\widehat{\overline{\rho}\overline{S}\overline{S}_{ij}^*}, \\ C_{dsm}=-\frac{L_{ij}^*M_{ij}}{2M_{ij}M_{ij}}, \end{cases} \tag{76}$$

where $L_{ij}=\widehat{\overline{\rho U_i}\,\overline{\rho U_j}}/\overline{\rho}-\widehat{\overline{\rho U_i}}\,\widehat{\overline{\rho U_j}}/\widehat{\overline{\rho}}$, $L_{ij}^*=L_{ij}-L_{kk}\delta_{ij}/3$, $\widetilde{S}_{ij}^*=\widetilde{S}_{ij}-\widetilde{S}_{kk}\delta_{ij}$, and $\widetilde{S}_{ij}=(\widetilde{U}_{i,j}+\widetilde{U}_{j,i})/2$, $|\widetilde{S}|=(2\widetilde{S}_{ij}\widetilde{S}_{ij})^{\frac{1}{2}}$, and $|\widehat{\widetilde{S}}|=(2\widehat{\widetilde{S}}_{ij}\widehat{\widetilde{S}}_{ij})^{\frac{1}{2}}$.

2.2 Dynamic coefficient for double time-relaxation kinetic model

In DtrKM, τ_{ij}^{sgs} is modeled by the gradient-type eddy viscosity model in Eq. (22), and the coefficient C_s is determined by

$$\begin{cases} L_{ij}^*=-2C_sM_{ij}, \\ M_{ij}=\widehat{\overline{\Delta}}\widehat{\overline{\rho}}\widehat{K}_{utke}^{\frac{1}{2}}\widehat{\widetilde{S}}_{ij}^*-\overline{\Delta}\overline{\rho}\widehat{K_{utke}^{\frac{1}{2}}\widetilde{S}_{ij}^*}, \\ C_s=-\frac{L_{ij}^*M_{ij}}{2M_{ij}M_{ij}}, \end{cases} \tag{77}$$

where $L_{ij} = \widehat{\overline{\rho}\widetilde{U}_i}\widehat{\overline{\rho}\widetilde{U}_j}/\overline{\rho} - \widehat{\overline{\rho}\widetilde{U}_i}\widehat{\overline{\rho}\widetilde{U}_j}/\widehat{\overline{\rho}}$, $L^*_{ij} = L_{ij} - L_{kk}\delta_{ij}/3$, and $\widehat{\overline{K}}_{utke} = \widehat{K}_{utke} + (\widehat{\widetilde{U}_k\widetilde{U}_k} - \widehat{\widetilde{U}}_k\widehat{\widetilde{U}}_k)/2$. When modifying the intrinsic turbulent Prandtl number $Pr_t = 1$ in DtrKM, the realistic turbulent Prandtl number can be computed dynamically as

$$\begin{cases} L_j = -C_s M_j / Pr_t, \\ M_j = \widehat{\overline{\Delta}}\widehat{\overline{\rho}}\widehat{\overline{K}}^{\frac{1}{2}}_{utke}\widehat{\widetilde{T}}_{,j} - \widehat{\overline{\Delta}\overline{\rho}K^{\frac{1}{2}}_{utke}\widetilde{T}_{,j}}, \\ Pr_t = -\frac{C_s M_j M_j}{L_j M_j}, \end{cases} \tag{78}$$

where $L_j = R(\widehat{\overline{\rho T}\,\overline{\rho U_j}}/\overline{\rho} - \widehat{\overline{\rho T}}\,\widehat{\overline{\rho U_j}}/\widehat{\overline{\rho}})$. To model the pressure-dilation transfer, following the series expansion [19], C_Π reads

$$\begin{cases} L_\Pi = C_\Pi M_\Pi, \\ M_\Pi = \widehat{\overline{\Delta}}^2\widehat{\overline{p}}_{,j}(\widehat{\overline{\rho}\widetilde{U}_k}/\widehat{\overline{\rho}})_{j,k} - \widehat{\overline{\Delta}^2\overline{p}_{,j}(\widetilde{U}_k)_{j,k}}, \\ C_\Pi = \frac{L_\Pi}{M_\Pi}, \end{cases} \tag{79}$$

where $L_\Pi = \overline{p}(\widehat{\overline{\rho}\widetilde{U}_k}/\overline{\rho})_{,k} - \widehat{\overline{p}}(\widehat{\overline{\rho}\widetilde{U}_k}/\widehat{\overline{\rho}})_{,k}$.

The coefficients $C_{\epsilon s}$ and $C_{\epsilon d}$ are obtained by the analogy between the grid-filter-level SGS stress and the resolved stress across the test filter level [50], where $L = CM$ instead of $L = C(M - \widehat{m})$. To model the solenoidal dissipation rate, $C_{\epsilon s}$ reads

$$\begin{cases} L_{\epsilon s} = \widehat{\overline{\mu}\widetilde{w}_i\widetilde{w}_i} - \widehat{\overline{\mu}}\widehat{\widetilde{w}}_i\widehat{\widetilde{w}}_i, \\ M_{\epsilon s} = \widehat{\overline{\rho}}\widehat{\overline{K}}^{\frac{3}{2}}_{utke}/\widehat{\overline{\Delta}}, \\ C_{\epsilon s} = L_{\epsilon s}/M_{\epsilon s}. \end{cases} \tag{80}$$

To model the dilational dissipation rate, $C_{\epsilon d}$ reads

$$\begin{cases} L_{\epsilon d} = 4\left[\widehat{\overline{\mu}\widetilde{U}^2_{k,k}} - \widehat{\overline{\mu}}\widehat{\widetilde{U}}^2_{k,k}\right]/3, \\ M_{\epsilon d} = \widehat{\overline{\rho}}^2\widehat{\overline{K}}^{\frac{5}{2}}_{utke}/(\gamma\widehat{\overline{p}}\,\widehat{\overline{\Delta}}), \\ C_{\epsilon d} = L_{\epsilon d}/M_{\epsilon d}. \end{cases} \tag{81}$$

Remark 1

For DCIT, the global dynamic coefficient is obtained through the ensemble average in the whole computational domain. In terms of TCPML, the local dynamic coefficient is obtained through the plane averaging in the streamwise and spanwise directions.

Remark 2

When modeling SGS pressure-dilation transfer, the dynamic denominator in C_Π may approach a pretty tiny value, which causes a large value for model coefficient C_Π. To smoothen the spurious behavior of C_Π, the C_Π is limited in a bound $[-0.1, 0.1]$ to guarantee the numerical robustness. When C_Π goes beyond the bound, it would be modified as $C_\Pi = C^{lim}_\Pi \cdot \mathrm{sign}(C_\Pi)$, where $C^{lim}_\Pi = 0.05$ and $\mathrm{sign}(\cdot)$ is the sign function. Both for DCIT

and TCPML, numerical tests indicate that the key statistical quantities are not sensitive to the C_{Π}^{lim}*, as long as the numerical simulations are stable.*

Remark 3

For macroscopic variable β*, the filtered macroscopic variable and Favre-filtered variable are denoted as* $\overline{\beta}$ *and* $\tilde{\beta}$ *in Eqs. (18) - (26) and Appendix 2, respectively. By default, macroscopic variable* β *in the rest part of this paper, such as the derivation of macroscopic governing equations from DtrKM in Appendix 1, represents resolved value without additional filtering symbols. Since resolved conservative variables on unresolved grids can be regarded as the filtered conservative variables, the corresponding Favre-filtered primitive variables also can be obtained. In summary, the* ***resolved variables*** *in the current paper can be treated as the customary* ***filtered variables*** *equivalently.*

Appendix 3 Connection between macroscopic variables and mesoscopic coefficients

The connection between the spatial derivatives of macroscopic flow variables and the expansion of turbulence equilibrium distribution function f^{eq} reads

$$\frac{\partial \boldsymbol{Q}}{\partial x_i} = \int \frac{\partial f^{eq}}{\partial x_i} \boldsymbol{\psi} \mathrm{d}\Xi \equiv \int a f^{eq} \boldsymbol{\psi} \mathrm{d}\Xi, \tag{82}$$

where a denotes the spatial mesoscopic coefficients in Eq. (33) as

$$a = \boldsymbol{a}^T \boldsymbol{\psi} = a_1 + a_2 u_1 + a_3 u_2 + a_4 u_3 + a_5 \left[\frac{1}{2} \left(u_1^2 + u_2^2 + u_3^2 + \xi^2 \right) + k_u \right] + a_6 k_u. \tag{83}$$

Equation (82) can be rewritten into the following linear system,

$$\frac{1}{\rho} \frac{\partial \boldsymbol{Q}}{\partial x_i} = \left(\frac{1}{\rho} \int \boldsymbol{\psi} \otimes \boldsymbol{\psi}^T f^{eq} \mathrm{d}\Xi \right) \boldsymbol{a} \triangleq \boldsymbol{M} \boldsymbol{a}. \tag{84}$$

Each component of $(a_1, ..., a_6)^T$ in Eq. (84) can be determined uniquely,

$$\begin{cases} a_6 = \frac{4}{\rho K_{utke}^2} B_5 - a_5, \\ a_5 = \frac{8\lambda^2}{\rho(N+3)} (B_4 - U_1 B_1 - U_2 B_2 - U_3 B_3 - B_5), \\ a_4 = \frac{2\lambda}{\rho} B_3 - U_3 a_5, \\ a_3 = \frac{2\lambda}{\rho} B_2 - U_2 a_5, \\ a_2 = \frac{2\lambda}{\rho} B_1 - U_1 a_5, \\ a_1 = \frac{1}{\rho} \frac{\partial \rho}{\partial x_i} - U_1 a_2 - U_2 a_3 - U_3 a_4 - E a_5 - K_{utke} a_6, \end{cases} \tag{85}$$

where

$$\begin{cases} B_1 = \frac{\partial(\rho U_1)}{\partial x_i} - U_1 \frac{\partial \rho}{\partial x_i}, \\ B_2 = \frac{\partial(\rho U_2)}{\partial x_i} - U_2 \frac{\partial \rho}{\partial x_i}, \\ B_3 = \frac{\partial(\rho U_3)}{\partial x_i} - U_3 \frac{\partial \rho}{\partial x_i}, \\ B_4 = \frac{\partial(\rho E)}{\partial x_i} - E \frac{\partial \rho}{\partial x_i}, \\ B_5 = \frac{\partial(\rho K_{utke})}{\partial x_i} - K_{utke} \frac{\partial \rho}{\partial x_i}. \end{cases} \tag{86}$$

For the temporal mesoscopic coefficient in Eq. (33), the relation between temporal derivatives of macroscopic variables and turbulence equilibrium distribution can be written as

$$\frac{\partial \boldsymbol{Q}}{\partial t} = \int \frac{\partial f^{eq}}{\partial t} \boldsymbol{\psi} \, \mathrm{d}\Xi \equiv \int A f^{eq} \boldsymbol{\psi} \, \mathrm{d}\Xi, \tag{87}$$

where

$$A = \boldsymbol{A}^T \boldsymbol{\psi} = A_1 + A_2 u_1 + A_3 u_2 + A_4 u_3 + A_5 \left[\frac{1}{2} \left(u_1^2 + u_2^2 + u_3^2 + \xi^2 \right) + k_u \right] + A_6 k_u. \tag{88}$$

The temporal derivatives of macroscopic variables can be given according to the compatibility condition as

$$\int \left(\frac{\partial f^{eq}}{\partial t} + u_i \frac{\partial f^{eq}}{\partial x_i} \right) \boldsymbol{\psi} \, \mathrm{d}\Xi = \boldsymbol{0}. \tag{89}$$

In a similar way, the above components $(A_1, ..., A_6)^T$ in Eq. (87) can be determined uniquely.

Appendix 4 Eigenstructure for characteristic reconstruction

The Jacobian matrix $\boldsymbol{J}$ for the flux $\boldsymbol{F}(\boldsymbol{Q})$ of the hyperbolic part in Eqs. (10)-(13) is given by

$$\boldsymbol{J} = \begin{pmatrix} 0 & 1 & 0 & 0 & 0 & 0 \\ \frac{\hat{\gamma}}{2}\boldsymbol{U^2} - U_1^2 & (3-\gamma)U_1 & -\hat{\gamma}U_2 & -\hat{\gamma}U_3 & \hat{\gamma} & -\hat{\gamma} \\ -U_1 U_2 & U_2 & U_1 & 0 & 0 & 0 \\ -U_1 U_3 & U_3 & 0 & U_1 & 0 & 0 \\ U_1\left(\frac{\gamma-2}{2}\boldsymbol{U^2} - \frac{c^2}{\gamma-1} - K_{utke}\right) & H - \hat{\gamma}U_1^2 + K_{utke} & -\hat{\gamma}U_1 U_2 & -\hat{\gamma}U_1 U_3 & \gamma U_1 & -\hat{\gamma}U_1 \\ -U_1 K_{utke} & K_{utke} & 0 & 0 & 0 & U_1 \end{pmatrix}, \tag{90}$$

where $H = \boldsymbol{U^2}/2 + c^2/(\gamma - 1)$, and $\hat{\gamma} = \gamma - 1$. The eigenvalues of the quasi one-dimensional system are

$$\lambda_1 = U_1 - c, \quad \lambda_2 = U_1, \quad \lambda_3 = U_1, \quad \lambda_4 = U_1, \quad \lambda_5 = U_1, \quad \lambda_6 = U_1 + c, \tag{91}$$

where c is the local sound speed. The matrix of the corresponding right eigenmatrix is

$$\boldsymbol{R} = \begin{pmatrix} 1 & 1 & 0 & 0 & 0 & 1 \\ U_1 - c & U_1 & 0 & 0 & 0 & U_1 + c \\ U_2 & U_2 & 1 & 0 & 0 & U_2 \\ U_3 & U_3 & 0 & 1 & 0 & U_3 \\ H - U_1 c + K_{utke} & \frac{1}{2}\boldsymbol{U^2} & U_2 & U_3 & 1 & H + U_1 c + K_{utke} \\ K_{utke} & 0 & 0 & 0 & 1 & K_{utke} \end{pmatrix}, \tag{92}$$

and the inverse matrix of $\boldsymbol{R}$ is given by

$$\boldsymbol{R}^{-1}=\frac{\hat{\gamma}}{2c^2}\begin{pmatrix} \frac{1}{2}\boldsymbol{U^2}+\frac{U_1c}{\hat{\gamma}} & -\left(U_1+\frac{c}{\hat{\gamma}}\right) & -U_2 & -U_3 & 1 & -1 \\ -\boldsymbol{U^2}+\frac{2c^2}{\hat{\gamma}} & 2U_1 & 2U_2 & 2U_3 & -2 & 2 \\ -\frac{2U_2c^2}{\hat{\gamma}} & 0 & \frac{2c^2}{\hat{\gamma}} & 0 & 0 & 0 \\ -\frac{2U_3c^2}{\hat{\gamma}} & 0 & 0 & \frac{2c^2}{\hat{\gamma}} & 0 & 0 \\ -\boldsymbol{U^2}K_{utke} & 2U_1K_{utke} & 2U_2K_{utke} & 2U_3K_{utke} & -2K_{utke} & 2K_{utke}+\frac{2c^2}{\hat{\gamma}} \\ \frac{1}{2}\boldsymbol{U^2}-\frac{U_1c}{\hat{\gamma}} & -U_1+\frac{c}{\hat{\gamma}} & -U_2 & -U_3 & 1 & -1 \end{pmatrix}. \tag{93}$$

Acknowledgements
Thank Prof. M.P. Wan at SUSTech, Dr. Z.Y. Wang and Dr. W. Xu at HKUST for helpful discussions. The authors would like to thank Taiyi supercomputers in SUSTech for providing high performance computational resources.

Authors' contributions
Guiyu Cao: Conceptualization, Methodology, Coding, Writing & Editing. Liang Pan: Conceptualization & Editing. Kun Xu: Funding acquisition, Conceptualization & Editing. Shiyi Chen: Funding acquisition, Conceptualization & Supervision. All authors read and approved the final manuscript.

Funding
Liang Pan was supported by the National Natural Science Foundation of China (12494543 and 12471364) and the Beijing Natural Science Foundation (1232012). Kun Xu was supported by the National Natural Science Foundation of China (91852114 and 11772281), and the National Numerical Windtunnel project. Shiyi Chen was supported by the Department of Science and Technology of Guangdong Province (2020B1212030001).

Data availability
Data will be made available on request.

Declarations

Competing interests
The authors declare that they have no known competing financial interests or personal relationships that could have appeared to influence the work reported in this paper.

Received: 30 April 2025 Revised: 24 June 2025 Accepted: 20 July 2025
Published online: 04 December 2025

References

1. Pope SB (2001) Turbulent flows. Meas Sci Technol 12(11):2020
2. Manabe S, Smagorinsky J, Strickler RF (1965) Simulated climatology of a general circulation model with a hydrologic cycle. Mon Weather Rev 93(12):769–798
3. Lilly DK (1967) The representation of small-scale turbulence in numerical simulation experiments. In: Goldstine HH (Ed) Proceedings of IBM Scientific Computing Symposium on Environmental Sciences, Yorktown Heights, 1967, pp 195–210
4. Sagaut P (2006) Large eddy simulation for incompressible flows: an introduction. Springer Berlin, Heidelberg
5. Garnier E, Adams N, Sagaut P (2009) Large eddy simulation for compressible flows. Springer, Dordrecht
6. Schumann U (1975) Subgrid scale model for finite difference simulations of turbulent flows in plane channels and annuli. J Comput Phys 18:376–404
7. Yoshizawa A, Horiuti K (1985) A statistically-derived subgrid-scale kinetic energy model for the large-eddy simulation of turbulent flows. J Phys Soc Jpn 54(8):2834–2839
8. Deardorff JW (1970) A numerical study of three-dimensional turbulent channel flow at large Reynolds numbers. J Fluid Mech 41(2):453–480
9. Germano M, Piomelli U, Moin P et al (1991) A dynamic subgrid-scale eddy viscosity model. Phys Fluids A 3(7):1760–1765
10. Moin P, Squires K, Cabot W et al (1991) A dynamic subgrid-scale model for compressible turbulence and scalar transport. Phys Fluids A 3(11):2746–2757
11. Lilly DK (1992) A proposed modification of the Germano subgrid-scale closure method. Phys Fluids A 4(3):633–635
12. Meneveau C, Lund TS, Cabot WH (1996) A Lagrangian dynamic subgrid-scale model of turbulence. J Fluid Mech 319:353–385
13. Wilcox DC (1998) Turbulence modeling for CFD, 2nd edn. DCW Industries, La Canada
14. Krajnović S, Davidson L (2002) A mixed one-equation subgrid model for large-eddy simulation. Int J Heat Fluid Flow 23(4):413–425
15. De Stefano G, Vasilyev OV, Goldstein DE (2008) Localized dynamic kinetic-energy-based models for stochastic coherent adaptive large eddy simulation. Phys Fluids 20(4):045102
16. Sarkar S, Erlebacher G, Hussaini MY et al (1991) The analysis and modelling of dilatational terms in compressible turbulence. J Fluid Mech 227:473–493

17. Yoshizawa A (1986) Statistical theory for compressible turbulent shear flows, with the application to subgrid modeling. Phys Fluids 29(7):2152–2164
18. Pomraning E, Rutland CJ (2002) Dynamic one-equation nonviscosity large-eddy simulation model. AIAA J 40(4):689–701
19. Chai X, Mahesh K (2012) Dynamic *k*-equation model for large-eddy simulation of compressible flows. J Fluid Mech 699:385–413
20. Cao G, Pan L, Xu K (2021) Three dimensional high-order gas-kinetic scheme for supersonic isotropic turbulence II: coarse-graining analysis of compressible Ksgs budget. J Comput Phys 439:110402
21. Bhatnagar PL, Gross EP, Krook M (1954) A model for collision processes in gases. I. Small amplitude processes in charged and neutral one-component systems. Phys Rev 94:511
22. Chapman S, Cowling TG (1970) The mathematical theory of non-uniform gases: an account of the kinetic theory of viscosity, thermal conduction and diffusion in gases, 3rd edn, vol 1. Cambridge University Press, Cambridge, pp 27–52
23. Xu K (2001) A gas-kinetic BGK scheme for the Navier–Stokes equations and its connection with artificial dissipation and Godunov method. J Comput Phys 171(1):289–335
24. Xu K (2015) Direct modeling for computational fluid dynamics: construction and application of unified gas-kinetic schemes. World Scientific, Singapore
25. Castro M, Costa B, Don WS (2011) High order weighted essentially non-oscillatory WENO-Z schemes for hyperbolic conservation laws. J Comput Phys 230(5):1766–1792
26. Hou S, Sterling J, Chen S et al (1996) A lattice Boltzmann subgrid model for high Reynolds number flows. arXiv preprint, arXiv:comp-gas/9401004
27. Chen H, Kandasamy S, Orszag S et al (2003) Extended Boltzmann kinetic equation for turbulent flows. Science 301(5633):633–636
28. Jiang J, Qian Y (2012) Implicit gas-kinetic BGK scheme with multigrid for 3D stationary transonic high-Reynolds number flows. Comput Fluids 66:21–28
29. Righi M (2016) A gas-kinetic scheme for turbulent flow. Flow Turbul Combust 97:121–139
30. Cao G, Su H, Xu J et al (2019) Implicit high-order gas kinetic scheme for turbulence simulation. Aerosp Sci Technol 92:958–971
31. Pan D, Zhong C, Li J et al (2016) A gas-kinetic scheme for the simulation of turbulent flows on unstructured meshes. Int J Numer Methods Fluids 82(11):748–769
32. Tan S, Li Q, Xiao Z et al (2018) Gas kinetic scheme for turbulence simulation. Aerosp Sci Technol 78:214–227
33. Luan P, Zhang H, Zhang J (2025) Constructing turbulence models using the kinetic Fokker-Planck equation. J Fluid Mech 1011:A44
34. Yang X, Xu K (2025) Wave-particle based multiscale modeling and simulation of non-equilibrium turbulent flows. arXiv preprint, arXiv:2503.07207
35. Fu S, Li Q (2006) Numerical simulation of compressible mixing layers. Int J Heat Fluid Flow 27(5):895–901
36. Liao W, Peng Y, Luo LS (2009) Gas-kinetic schemes for direct numerical simulations of compressible homogeneous turbulence. Phys Rev E 80(4):046702
37. Liao W, Peng Y, Luo LS (2010) Effects of multitemperature nonequilibrium on compressible homogeneous turbulence. Phys Rev E 81(4):046704
38. Kumar G, Girimaji SS, Kerimo J (2013) WENO-enhanced gas-kinetic scheme for direct simulations of compressible transition and turbulence. J Comput Phys 234:499–523
39. Cao G, Pan L, Xu K (2019) Three dimensional high-order gas-kinetic scheme for supersonic isotropic turbulence i: criterion for direct numerical simulation. Comput Fluids 192:104273
40. Samtaney R, Pullin DI, Kosović B (2001) Direct numerical simulation of decaying compressible turbulence and shocklet statistics. Phys Fluids 13(5):1415–1430
41. Sandham ND, Reynolds WC (1991) Three-dimensional simulations of large eddies in the compressible mixing layer. J Fluid Mech 224:133–158
42. Vreman B, Geurts B, Kuerten H (1997) Large-eddy simulation of the turbulent mixing layer. J Fluid Mech 339:357–390
43. Pantano C, Sarkar S (2002) A study of compressibility effects in the high-speed turbulent shear layer using direct simulation. J Fluid Mech 451:329–371
44. Pan L, Xu K, Li Q et al (2016) An efficient and accurate two-stage fourth-order gas-kinetic scheme for the Euler and Navier–Stokes equations. J Comput Phys 326:197–221
45. Wang J, Yang Y, Shi Y et al (2013) Cascade of kinetic energy in three-dimensional compressible turbulence. Phys Rev Lett 110(21):214505
46. Xu K, Huang JC (2010) A unified gas-kinetic scheme for continuum and rarefied flows. J Comput Phys 229(20):7747–7764
47. Vreman B, Geurts B, Kuerten H (1994) Realizability conditions for the turbulent stress tensor in large-eddy simulation. J Fluid Mech 278:351–362
48. Xu K, He X, Cai C (2008) Multiple temperature kinetic model and gas-kinetic method for hypersonic non-equilibrium flow computations. J Comput Phys 227(14):6779–6794
49. Menon S, Kim WW (1996) High Reynolds number flow simulations using the localized dynamic subgrid-scale model. In: 34th Aerospace Sciences Meeting and Exhibit, Reno, 15-18 January 1996
50. Cao G, Liu H, Xu K (2018) Physical modeling and numerical studies of three-dimensional non-equilibrium multitemperature flows. Phys Fluids 30(12):126104
51. Cao G, Pan L, Xu K (2022) High-order gas-kinetic scheme with parallel computation for direct numerical simulation of turbulent flows. J Comput Phys 448:110739
52. Li J, Du Z (2016) A two-stage fourth order time-accurate discretization for Lax–Wendroff type flow solvers I. Hyperbolic conservation laws. SIAM J Sci Comput 38(5):A3046–A3069
53. Pan L, Xu K (2020) High-order gas-kinetic scheme with three-dimensional WENO reconstruction for the Euler and Navier-Stokes solutions. Comput Fluid 198:104401

54. Arun S, Sameen A, Srinivasan B et al (2019) Topology-based characterization of compressibility effects in mixing layers. J Fluid Mech 874:38–75
55. Sandham ND (1989) A numerical investigation of the compressible mixing layer. Dissertation, Stanford University
56. Toro EF (2009) Riemann solvers and numerical methods for fluid dynamics: a practical introduction. Springer Berlin, Heidelberg
57. Chen S, Xia Z, Pei S et al (2012) Reynolds-stress-constrained large-eddy simulation of wall-bounded turbulent flows. J Fluid Mech 703:1–28
58. Chen L, Xiao Z, Shi Y et al (2017) Constrained large-eddy simulation of supersonic turbulent boundary layer over a compression ramp. J Turbul 18(8):781–808
59. Cramer MS (2012) Numerical estimates for the bulk viscosity of ideal gases. Phys Fluids 24(6):066102

Publisher's Note